Pre-print:
M. La Cerva, L. Gurreri, A. Cipollina, M. Ciofalo, G. Micale, *Modelling and cost analysis of hybrid systems for seawater desalination: electromembrane pre-treatments for Reverse Osmosis*, Desalination, 467 (2019) 175-195, https://doi.org/10.1016/j.desal.2019.06.010

Modelling and cost analysis of hybrid systems for seawater desalination: electromembrane pre-treatments for Reverse Osmosis

Mariagiorgia La Cerva, Luigi Gurreri, Andrea Cipollina*, Alessandro Tamburini, Michele Ciofalo, Giorgio Micale

Dipartimento di Ingegneria

Università degli Studi di Palermo, Palermo, Italy

*corresponding author, e–mail: andrea.cipollina@unipa.it

Abstract

The need to reduce energy consumption in seawater Reverse Osmosis (RO) process has pushed research towards the development of new hybrid systems in which, for example, other membrane processes can be used to pre-treat seawater. Electrodialysis (ED) and Reverse Electrodialysis (RED) can act as a dilution step before seawater enters the RO unit, thus leading to an important energy saving in RO. In this work, two coupled models are proposed for the RED-RO and ED-RO systems. Each process model was validated. Then a sensitivity analysis was performed to assess the effect of the integration on the overall process cost saving. The analysis was performed by changing ED or RED voltage and RO pressure and considering eight different cost scenarios. The performance of the hybrid system was compared with the stand-alone seawater RO process. Competitive scenarios were found especially for the RED-RO case, by optimizing the dilution extent, with significant cost saving and promising potentials for future industrial implementation.

Keywords: *hybrid process; electromembrane process; assisted reverse electrodialysis; energy consumption; process intensification; cost.*

1. Introduction

In order to meet the growing demand of high quality water supply, desalination has been largely implemented over the past 3-4 decades. The cumulative contracted capacity of desalination reached almost 100 million m^3/day in 2016 [1]. Water desalination can be practised by thermal or membrane processes, among which reverse osmosis (RO) has become the dominant technology [2,3], covering 63% of the world desalination market [4]. In all RO plants, high pressure seawater feed pumps supply the pressure necessary to generate a positive flux of fresh water through the membrane [5]. Specific energy consumption in seawater reverse osmosis (SWRO) plants has declined dramatically in the past 40 years: better membranes, improvements in pump efficiency and the use of energy recovery devices (ERD) have allowed values of 3–4 kWh/m^3 or even lower to be obtained [6]. Nevertheless, energy consumption is still the major operational cost of SWRO process [7].

In order to enhance process performance and reduce energy consumption, researchers are studying new nanotube and nanocomposite membranes [8] and new design of the pressure vessels [9], though this cannot overtake the thermodynamic constrain related to the need of exceeding the osmotic pressure of the stream flowing in the feed channel to obtain a permeate. Thus, some new directions for process intensification look at the implementation of hybrid schemes for the combined production of water and energy [10,11] or for the pre-dilution of seawater aiming at the reduction of pumping power requirements [7,12].

Under this respect, two different approaches have been proposed. The first is based on the use of “osmotic dilution” steps, which require a low-salinity sink stream, such as reclaimed water from a waste water treatment plant. Dilution is obtained by the transport of water from the sink stream into the feed seawater, when osmotic membranes are adopted (e.g. Pressure Retarded Osmosis, Forward Osmosis and Pressure Assisted Osmosis [13–15], see Figure 1a), or, *vice*

versa, by the transport of salt from the feed seawater into the sink stream, when ion-exchange membranes are used (e.g. Reverse Electrodialysis, short-circuit Reverse Electrodialysis and Assisted Reverse Electrodialysis [16–18], see Figure 1b).

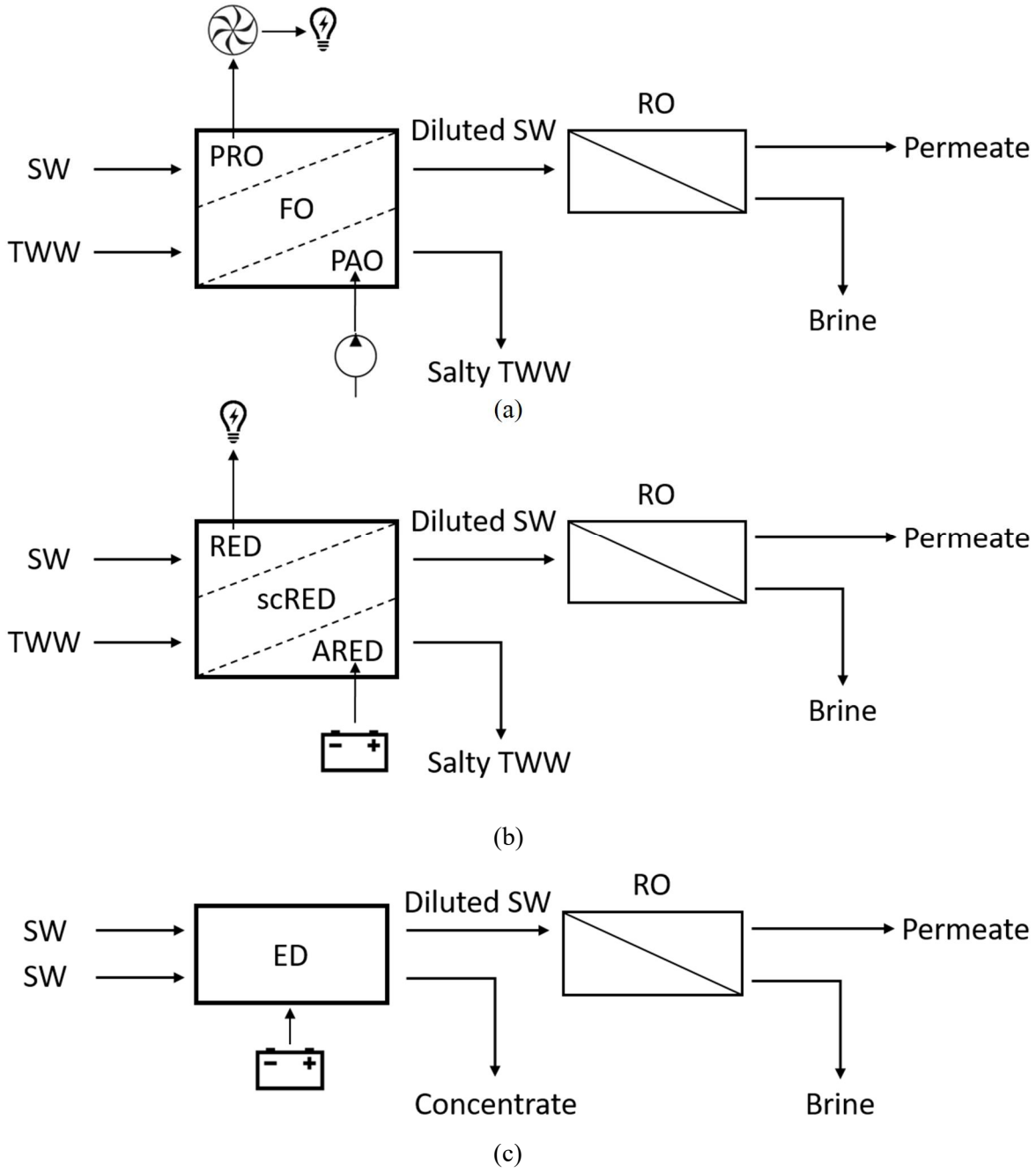

Figure 1. Schematic diagrams of the possible hybrid system configurations where Reverse Osmosis is coupled with a) Pressure Retarded Osmosis (PRO), Forword Osmosis (FO) or Pressure Assisted Osmosis (PAO); b) Reverse Electrodialysis (RED), short-circuit Reverse Electrodialysis (scRED) or Assisted Reverse Electrodialysis (ARED); c) Electrodialysis (ED).

The second approach is based on coupling RO with an Electrodialysis (ED) pre-dilution step, see Figure 1c. In this case, ED has the theoretical advantage of requiring lower specific energy for the removal of salt from high salinity streams compared to RO [19,20].

1.1. Osmotic Dilution technologies coupled with RO

Among "osmotic dilution" processes, Reverse Electrodialysis (RED) represents the most appealing for actual applications with reclaimed waters [16,18]. RED is a membrane process able to convert a salinity gradient into electrical energy by performing a partial mixing of two streams, so that the stream at high concentration, e.g. seawater, exits the RED unit with a lower concentration [21,22]. A RED unit consists of repeated periodic elements (cell pair) made by a cation and an anion exchange membrane, and two channels usually secured by polymeric net spacers. The presence of selective cation/anion exchange membranes forces the direction of ions movement from the concentrate to the dilute compartment so that a net electrical current is formed, while the electrical potential difference arising at each membrane/solution interface leads to the generation of an electromotive force, making this "membrane pile" a real power generator. Operational modes of RED are typically aimed at the generation of a maximum power, which requires the use of an external load resistance equal to the stack internal resistance. However, reducing the external load resistance, electrical current can increase until a maximum value in short-circuit conditions.

In hybrid arrangements with RO (Figure 1b), the RED process, besides reducing the energy consumption by producing green energy, can be used as a pre-treatment, reducing the feed salinity (i.e. the pressure level required for pumping in RO) or can be integrated with existing desalination plants using their outlet brine as the high salinity feed and providing also a dilution strategy for brine disposal [23].

Li *et al.* [18] explored both concepts in different configurations of RED and RO integration by using a simple lumped parameters model. Considering spacerless channels in RED under batch operations, they first studied the effects of the external load and of the concentration and volume of the dilute solution on the energy harvested and on the outlet concentration of the saline stream. The optimized operating conditions, which maximise the specific energy harvested and minimize the discharge time, were found for a low to high salinity ratio close to 0.01, an external load equal to the initial internal resistance and a volumetric ratio of the low to the high salinity solution of 2. This optimized design for the RED process was then combined with the RO process for which ideal membranes and uniform hydraulic pressure were considered. The authors observed that the RED-RO configuration is more effective in reducing the specific energy consumption compared to the RO-RED design. Moreover, arranging the RED process as a pre-treatment, reduces the risk of scaling for RO, since some divalent ions (Ca^{2+} and Mg^{2+}) can partially be removed. Also more complex schemes were simulated, showing promising results in reducing the energy consumption. However, the authors did not investigate the full optimisation of the integrated system, which may lead to very different "optimal" operating conditions compared to what was found by optimising the stand-alone RED and RO units.

More recently, Mei *et al.* [24] experimentally observed that the power density harvested from RED process can be increased if the sink stream, at low concentration, has concentration between 0.01 and 0.02 M, typical of effluents from treated municipal waste water, or when the high concentration stream has concentration from 0.6 to 2 M, typical of brine from RO. From these results, they proved that RED can be coupled with RO both as a pre-treatment and a post-treatment. However, they did not study the integrated system and a cost analysis is missing.

Other studies only focused on the role of RED process as a post-treatment to reduce the concentration of the brine produced in RO or other industrial processes, before discharging it, producing electric energy at the same time [11,25,26].

As reported in Figure 1b, another pre-dilution option is the Assisted Reverse Electrodialysis (ARED) process. In ARED an additional external voltage is applied in order to increase the stack electrical current (and consequently, the salt flux from seawater to the sink stream) above the short-circuit condition.

Vanoppen et al. [17,27] have proposed a hybrid scheme, consisting of an ARED stage followed by a brackish water RO (BWRO). The authors carried out experiments in order to characterize the ARED stack and then, considering the ARED-RO combination, they observed that, under certain operating conditions, an energy consumption reduction is possible. The economic analysis showed that the ARED-RO coupling was competitive with the stand-alone SWRO when the price of the ion exchange membranes (IEMs) was lower than 10 €/m^2.

1.2. Electrodialysis coupled with RO

A different integration scheme for seawater RO desalination is the coupling with an Electrodialysis (ED) unit. ED is typically adopted for brackish water desalination [28–30], though it has been recently proposed also for seawater desalination [31,32]. With reference to this latter case, ED can be coupled to RO for pre-diluting the feed seawater, thus reducing the operating pressure of RO (Figure 3c).

Galama *et al.* [33] studied experimentally the pre-desalination of seawater by ED. Supported by literature data on the energy consumption of BWRO systems, they found that current densities higher than 50 A/m^2 led to overall energy consumptions of the ED-BWRO lower than those of the stand-alone ED. The authors claimed the potential reduction of energy consumption also with respect to SWRO. However, no comparison with conventional stand-alone SWRO and no data supporting this conclusion were reported. Moreover, only energy costs are considered, which leads to possible misleading conclusions. McGovern *et al.* [19,20] assessed

the ED desalination performance by letting the feed salinity vary and they found the partial desalination of highly concentrated brackish waters as the most cost effective application, thus envisioning a possible use in ED-BWRO coupled treatments. The performance of an ED-BWRO real plant was tested for brackish water (2000-4000 ppm) desalination in domestic applications [34], showing promising results in increasing the recovery of produced water.

To the best of our knowledge, the only cost analysis presented so far on the ED-RO coupling has been performed by Post *et al.* [35]. They considered a theoretical ED spacerless unit, with ideal membranes (perfectly ion-selective, no transport of co-ions and water) and a low membrane cost (5 €/m^2). Under these assumptions, considering a limited range of operating conditions and considering theoretical energy consumptions, the ED-BWRO configuration was shown to be competitive with respect to SWRO.

For the sake of completeness, we mention that other coupling solutions presented in the literature concern the application of RO-ED systems, i.e. hybrid processes where the RO retentate brine is fed to a following ED step (in more or less complex schemes which may involve recirculations), e.g. for valorisation of reverse osmosis brines [36–39].

1.3. Aim of the work

The above literature review shows that schemes of hybridization in which electromembrane processes are used to valorise the brine produced in RO are very promising because they allow the diluted brine to be discharged with less environmental damages and/or they can also produce electricity. Concerning the use of electromembrane processes as pre-dilution steps for RO, a few works show the potential benefits of this integrations. However, the analysis reported are theoretical or based on simplified models, while a comparison with the standard stand-alone SWRO is not reported and cost analysis is often missing.

In this work, a comprehensive simulation tool was developed in order to perform a sensitivity analysis of the operation of hybrid schemes for (A)RED-RO and ED-RO processes combinations. The simulation tool was adopted to analyse the influence of operating parameters and operational strategies on the cost saving of the hybrid systems compared to stand-alone SWRO, identifying promising operational ranges and schemes.

2. Modelling

2.1. Electromembrane processes model

The ED/RED model here adopted can be used for the three electromembrane processes considered in this paper. It uses a one-dimensional representation of the stack, but it includes also local results from 3-D Computational Fluid Dynamics (CFD) simulations (friction coefficients [40–42], mass transfer coefficients [43,44], and Ohmic resistances). This coupling between CFD and a one-dimensional model was already presented in previous works [45,46].

The mass balance equations take into account osmotic, electro-osmotic and diffusive fluxes across the membranes. Ohmic losses, membrane potentials and concentration polarization phenomena are considered to compute the external voltage ΔV_{ext}.

With reference to Figure 2a, which shows a generic cell pair within a stack, the electric current I is assumed to be positive if directed from 1 to 2 through the stack (i.e. $I > 0$ for ED, $I < 0$ for RED and ARED); similarly, the external voltage ΔV_{ext} is positive if $V_1 > V_2$.

The three possible working modes (Electrodialysis, or ED; Reverse Electrodialysis, or RED; and Assisted Reverse Electrodialysis, or ARED) are qualitatively illustrated in Figure 2b, which reports ΔV_{ext} against I, and Figure 2c, which reports the power (generated or consumed) against I. The boundary between ED and RED is the Open Circuit condition (OC), in which ΔV_{ext} =

OCV and I =0. This occurs when in ED the feed solutions have different concentrations as in RED. The boundary between RED and ARED is the short circuit RED condition (scRED), in which ΔV_{ext} =0 and $I = I_{SC}$.

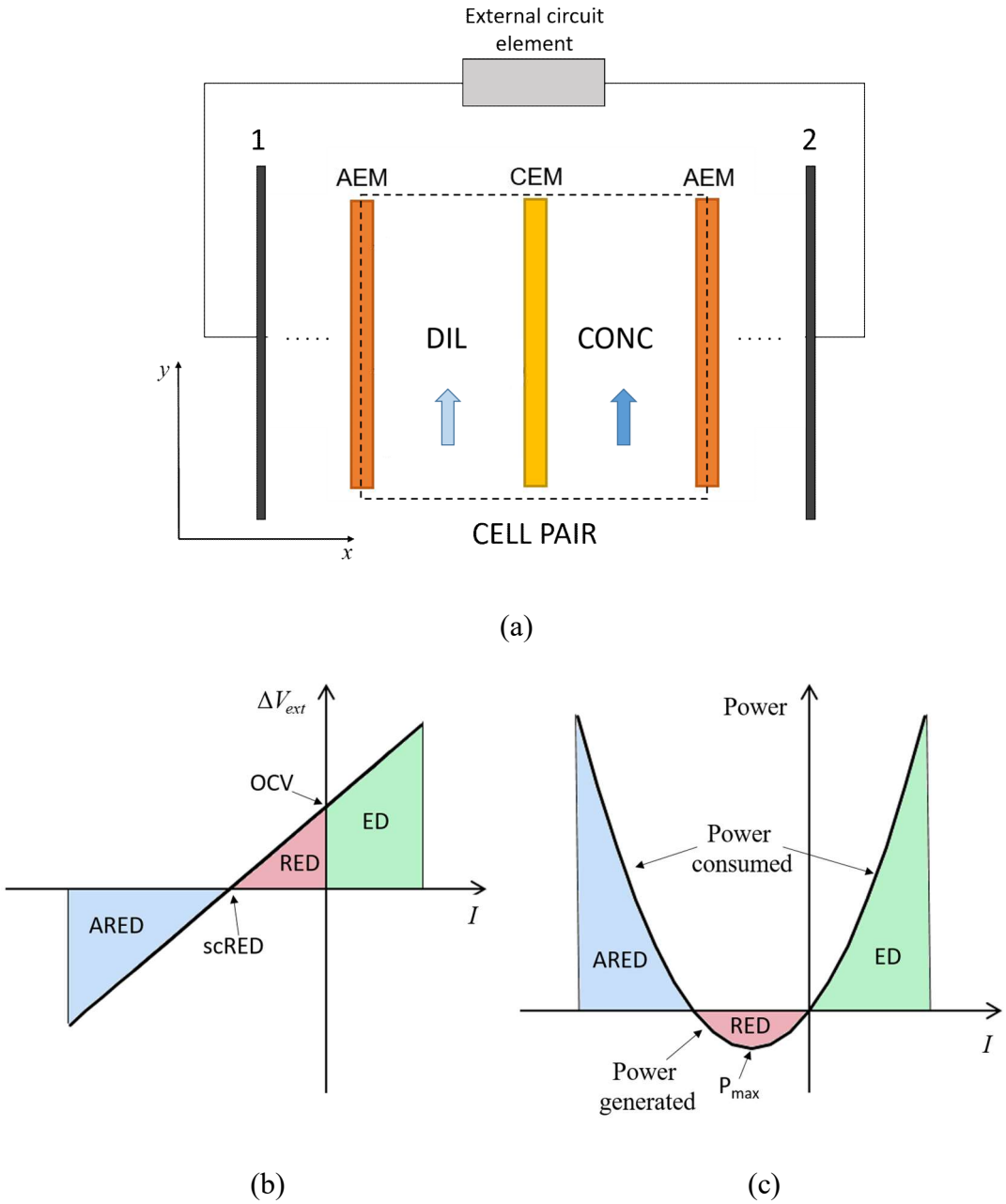

Figure 2. (a) Schematic representation of a cell pair; electrodes (1) and (2) are shown. The grey block indicates a passive or an active circuit element depending on the working mode. (b) Voltage-current curves; (c) power -current curves.

Table 1. Signs of current and voltage and role of the electrodes in different working modes, with reference to the scheme of Figure 2a.

Process	**Electrode 1**	ΔV_{ext}	***i* (direction)**	**Electrode 2**	**External circuit element**
ARED	Cathode (-)	< 0	< 0 (←)	Anode (+)	Generator
RED	Cathode (+)	> 0	< 0 (←)	Anode (-)	Resistance
ED	Anode (+)	> 0	> 0 (→)	Cathode (-)	Generator

Note that, according to the working conditions, each electrode (1 or 2) may be positive or negative and may play the role of anode (where oxidation reactions occur) or cathode (where reduction reactions occur). In particular, as summarized in Table 1:

- the positive electrode is the anode in ED and ARED while it is the cathode in RED;
- the negative electrode is the cathode in ED and ARED, while it is the anode in RED.

All the equations of the model, valid for all possible working modes, are reported in the Appendix. The model was implemented in a MS Excel™ spreadsheet integrated with VBA macros.

The model was validated in ED and RED conditions in previous works [45,46] and was additionally validated in ARED operating conditions by comparison with original experimental data purposely collected in a laboratory test-rig. Experiments were carried out in a parallel flow RED unit (REDstack BV, The Netherlands), with 10 cell pairs of active area equal to 10×10 cm^2. The stack was equipped with membranes supplied by Fujifilm Manufacturing Europe BV (The Netherlands), whose properties are reported in Table 2, and woven spacers (Deukum GmbH, Germany), 270 μm thick, with pitch to height ratio l/H = 2 and a porosity of 75%. The electrode rinse solution was prepared from deionized water adding 0.3 M $K_3Fe(CN)_6$, 0.3 M

$K_4Fe(CN)_6 \cdot 3H_2O$ and 0.25 M NaCl. Feed solutions were prepared with deionised water and technical grade NaCl, with concentrations from 0.5 to 2 g/l for the dilute feed and 35 g/l for the concentrate. The same inlet fluid velocity of 0.5 cm/s was imposed in the concentrate and dilute compartment.

The electrode rinse solution and feed solutions were circulated by peristaltic pumps (Masterflex Cole-Palmer). Inlet/outlet conductivities were measured by a laboratory conductivity-meter (WTW 340i). A laboratory stabilized power supply (Elektro-Automatic GmbH, Germany) was used to apply the current under galvanostatic mode, allowing also the measurement of the stack voltage.

Table 2. Properties of the FUJIFILM Type 10 ion exchange membranes (data provided by manufacturer).

	Permselectivity[a] [%]	Water permeability [ml/m^{2}hbar]	Salt diffusion permeability [m^2/s]	IEC [meq/g]	Resistance[b] [Ω cm^2]	Thickness (dry) [µm]	Thickness (wet) [µm]
AEM	97	8.0	4e-12	2.85	1.77	120	130
CEM	98	8.0	4e-12	2.9	1.89	120	130

[a] Based on electric potential measured over the membrane between 0.05 M and 0.5 M KCl solutions at 25°C.

[b] Measured in 2 M NaCl solution at 25°C.

In Figure 3 experimental data and simulation results are reported for tests at: a) 35 – 0.5 g/l and b) 35 – 2 g/l. The external voltage and the outlet concentrations from the dilute and the concentrate compartments are plotted as a function of the current density. At $i = 0$, the open circuit voltage is measured and this is higher when the ratio between the concentrations (35 and 0.5 g/l) is higher (Figure 3a). As explained in Figure 2b, when the current reaches the short-circuit value, the external voltage is zero. In ARED, in order to have currents higher than the short-circuit value, an external negative voltage must be applied. At increasing current densities, the external voltage increases (in absolute value) as well as the dilute outlet concentration, while the concentrate outlet salinity decreases.

The model results, represented with dashed lines, are in good agreement with experiments, though the model slightly overestimates the current density, likely due to some undersetting of the IEMs resistance values, while the salt fluxes are slightly underestimated. Such deviations are, however, acceptable and always in the conservative direction for our purposes (investigate the effectiveness of a pre-dilution step in hybrid schemes).

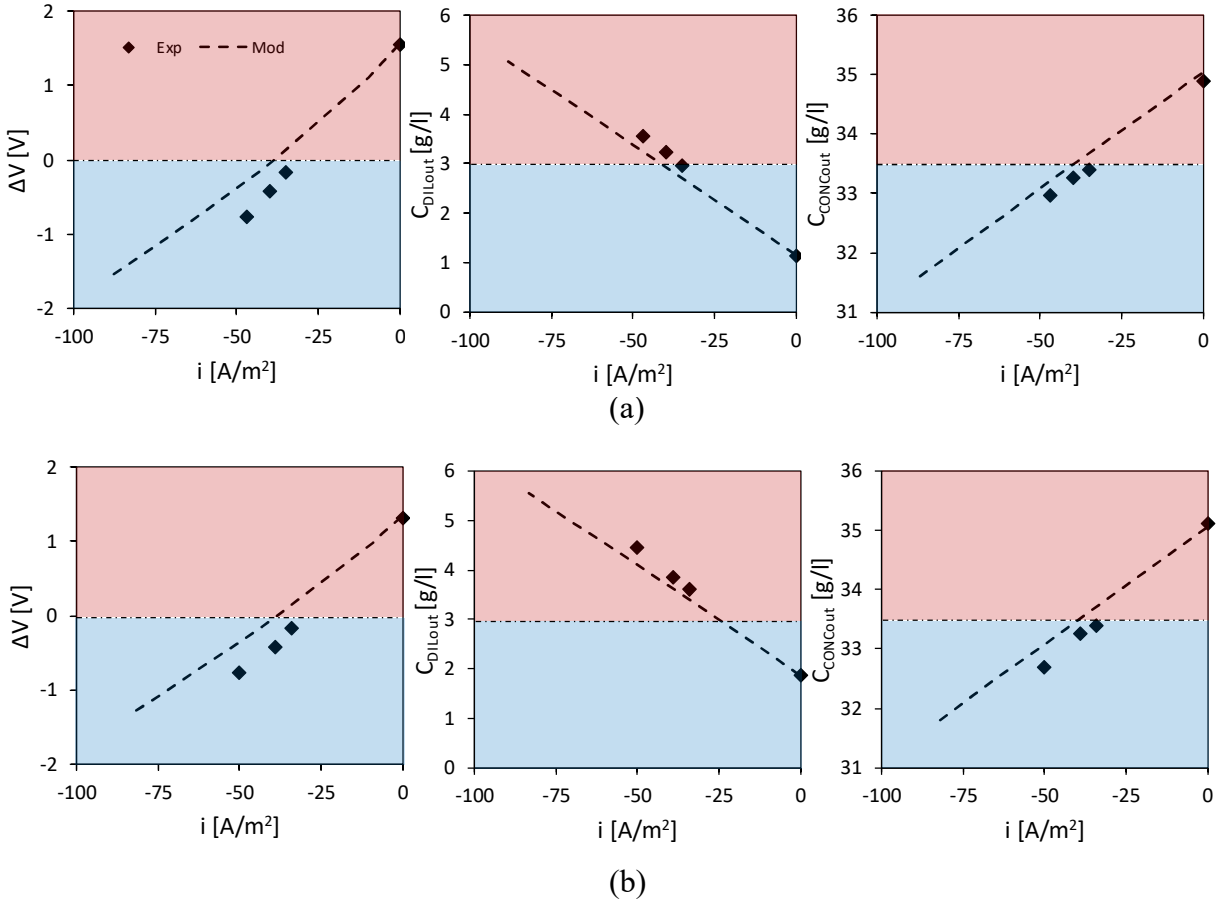

Figure 3. Comparison of experimental data (diamonds) and model predictions (dashed lines) for ARED operation. The external voltage (left column), the dilute (middle column) and concentrate (right column) outlet concentrations are reported as a function of current density. a) 35 g/l and 0.5 g/l inlet feed concentrations. b) 35 g/l and 2 g/l inlet feed concentrations. Fluid velocity is 0.5 cm/s for both solutions.

2.2. RO model

The model adopted for the RO process is a lumped parameter model, in which average concentrations and pressure in each RO module are considered to compute water and salt fluxes,

while variations along the modules of each pressure vessel (PV) are considered. Another simplifying assumption is that the pressure drops in the permeate channel are neglected.

Under these assumptions and with reference to Figure 4, which shows an example of a typical series arrangement of RO spiral-wound modules inside a PV, the mass balance equations in the *i*-th module can be written as:

$$Q_r^i = Q_f^i - Q_p^i \tag{1}$$

$$C_r^i Q_r^i = C_f^i Q_f^i - C_p^i Q_p^i \tag{2}$$

where Q_r^i is the retentate flow rate, Q_f^i is the feed flow rate, Q_p^i is the permeate flow rate, C_r^i, C_f^i and C_p^i are the salt concentrations in the retentate, in the feed and in the permeate, respectively.

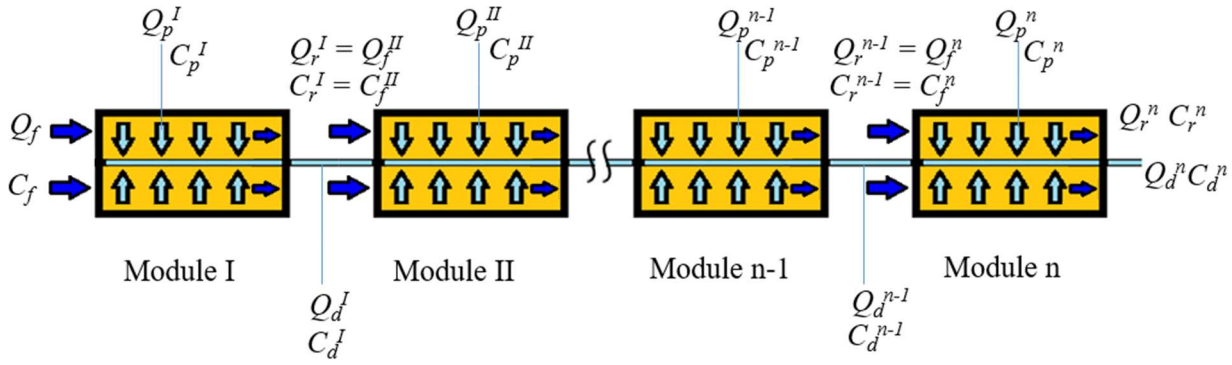

Figure 4. Sketch of an RO pressure vessel with *n* spiral wound membrane elements in series.

The permeate concentration (C_p^i) can be obtained from the salt molar flux (N_s^i) expression:

$$N_s^i = B\left(C_{f,avg}^i - C_p^i\right)/M_S \tag{3}$$

where B is the salt permeability constant, M_S is the molar mass of salt (in this case NaCl at 25 °C), while $C_{f,avg}^i$ and C_p^i are the average concentrations in the feed and in the permeate (expressed in g/l), respectively.

The water flux (J_W^i) and the permeate flow rate (Q_p^i) are functions of the water permeability constant, A, and the net driving force, according to Eq. (4):

$$Q_p^i = J_W^i S = A\left[P_{avg}^i - \left(\pi_f^i - \pi_p^i\right)\right]S \tag{4}$$

in which P_{avg}^i is the feed channel average pressure, π_f^i and π_p^i are the osmotic pressures of the feed (considering the average concentration in the channel) and the permeate, calculated by the Van't Hoff equation.

Since the average concentration ($C_{f,avg}^i$) depends on the permeate flow rate (Q_p^i) and this latter, in its turn, depends on $C_{f,avg}^i$ (as it affects the osmotic pressure Π_f^i), an iterative calculation is necessary to solve the set of equations.

The permeate is collected in the permeate duct, where its flow rate is added to that produced in all previous modules, while the concentration is obtained by a weighted average of the outlet concentrations from the previous modules, where the weights are the relevant flow rates. At the outlet of the pressure vessel, the flow rate (Q_d^n) and the salt concentration (C_d^n) of the permeate are:

$$Q_d^n = \sum_{i=1}^{n} Q_p^i \tag{5}$$

$$C_d^n = \frac{\sum_{i=1}^{n} C_p^i Q_p^i}{Q_p^n} \tag{6}$$

The outlet pressure in the *i*-th module is calculated as the inlet pressure minus the frictional losses:

$$P_r^i = P_f^i - \Delta P^i \tag{7}$$

Considering only the distributed frictional losses along the module, these can be estimated by the Darcy-Weisbach equation:

$$\Delta P^i = f \frac{L}{D_h} \rho^{SOL} \frac{U^2}{2} \tag{8}$$

where f is the friction factor, L is the module length, D_h is the channel hydraulic diameter assumed equal to twice the channel thickness, ρ^{SOL} is the density of the solution fed into the module and u is the void velocity, i.e. the velocity which would yield the given flow rate if the channel were spacerless.

The friction factor depends on the spacer geometry and on the Reynolds number. In regard to the spacer geometry, in the feed channel of an RO module, usually non-woven spacers are adopted [47–49]. Due to the lack of detailed data on the spacer geometry adopted in the commercial RO modules considered in this work, we used a friction factor value obtained from previous CFD simulations of overlapped spacers reported in [42]. In the range of the Reynolds numbers investigated here (100-300), the friction factor for the overlapped spacer with an orientation of 45° with respect to the flow, can be estimated as $f \approx 10 \cdot (96/Re)$.

The RO model described was implemented in a MS Excel™ spreadsheet and solved by macros.

Since a validation with experimental results was not possible, we compared our model with the theoretical predictions of two widely used commercial codes provided by DOW Chemical Company: ROSA, a user-friendly program for the RO module design, and its evolution, the more recently developed WAVE software [50].

In all simulations we assumed one PV with seven modules, all of the same type, which guarantee for all cases the achievement of the target permeate concentration (lower than 0.5 g/l). The modules were selected among three products offered by DOW Chemical, whose main features are reported in Table 3.

Table 3. Properties of RO modules by DOW Chemical [51–53].

	BW30HR-440i	**SEAMAXX**	**SW30XHR-440i**
Active area [m^2]	41	41	41
Length [m]	1.016	1.016	1.016
Channel thickness [mm]	0.7112	0.7112	0.7112
Permeate Flow rate [m^3/day]	48 [a]	64.4 [b]	23 [b]
Salt Rejection [%]	99.4 [a]	99.7 [b]	99.82 [b]
A [l/(m^2h bar)]†	3.581	2.424	0.938
B [l/(m^2h)]†	0.294	0.197	0.0458

[a] Values based on the following test conditions: 2,000 ppm NaCl, 15.5 bar, 25°C, pH 8 and 15% recovery.

[b] Values based on the following test conditions: 32,000 ppm NaCl, 55 bar, 25°C, pH 8 and 8% recovery.

† Values calculated from the modules' features reported in data sheets.

In Figure 5, the comparison between the model here presented and the commercial codes ROSA and WAVE is reported for the case of a single PV with seven SW30XHR-440i modules. The inlet flow rate was set equal to 10 m^3/h with a concentration of 32000 ppm and the feed pressure was imposed equal to 40 bar. Figure 5 shows that our model predictions are in very good agreement with those of the two commercial codes, with only a small overestimation of the permeate concentration.

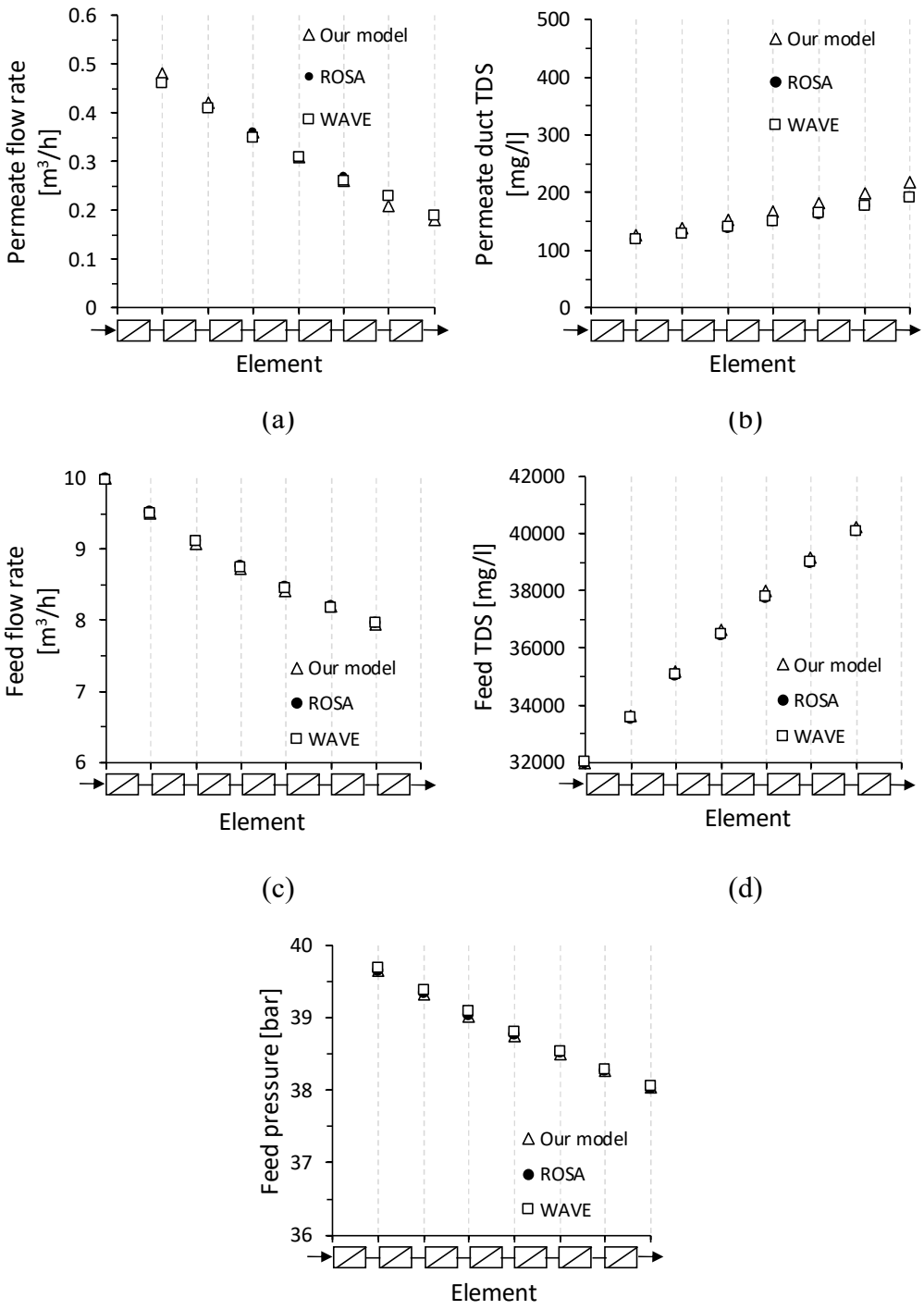

Figure 5. Comparison between the RO model presented in this work (empty triangles) and predictions of ROSA (solid circles) and WAVE (empty squares) softwares. Flow rates and TDS for feed and permeate duct are reported as a function of the elements. The feed pressure is also reported. Simulations were conducted with RO module SW30XHR-440i, inlet flow rate of 10 m^3/h, inlet concentration of 32000 ppm and feed pressure of 40 bar.

3. Simulation strategy and settings

3.1. (A)RED-RO and ED-RO integrated process schemes

Simulations were performed fixing feed seawater concentration of 30 g/l and a flow rate of 346 m^3/day related to the velocity and number of cell pairs of the pre-treatment dilution units (see Table 4). A concentration target equal or lower than 500 ppm for the final permeate produced was fixed for all simulations. The electrochemical pre-treatment of the (A)RED-RO coupled system was fed with a low salinity stream (e.g. treated waste water) at 1 g/l. For (A)RED and ED processes, co-current stacks of 0.5 x 0.5 m^2 were simulated. A spacer thickness of 160 μm was considered for the dilute and concentrate compartments. As a reference case (referred to as Case_A, see Table 4), an electromembrane plant with 2500 cell pairs and an inlet fluid velocity of 2 cm/s, corresponding to a residence time of 25 s, was considered. A second configuration with 5000 cell pairs (referred to as Case_B), with an inlet fluid velocity of 1 cm/s (corresponding to a residence time of 50 s) was also simulated. A flow ratio of 1 was fixed for the two streams entering the pre-treatment unit.

Table 4. Features of the electromembrane plant (ARED, RED or ED).

	N° of cell pairs	**Inlet fluid velocity [cm/s]**	**Residence time [s]**
Case A	2500	2	25
Case B	5000	1	50

The areal blank resistance, related to the electrode compartments, was set equal to $2 \cdot 10^{-3}$ Ω m^2. The efficiencies of the pump and of the Energy Recovery Device (ERD) were both assumed equal to 0.75 for the integrated process scheme.

A sensitivity analysis was performed by changing the external voltage in the (A)RED and ED processes. The maximum value of voltage under RED conditions was that maximising the power provided. The same absolute value (with negative sign) was set as the maximum voltage for the ARED process while 7 intermediate values were set, including the Open Circuit condition ($\Delta V=0$), as indicated in Table 5.

Table 5. Values of external voltage in the electromembrane pre-treatment chosen for the sensitivity analysis.

RED	$\Delta V^* = \Delta V \rightarrow P_{max}$ in RED
	$\Delta V = \Delta V^*/2$
	$\Delta V = \Delta V^*/3$
	$\Delta V = \Delta V^*/5$
Short circuit RED	$\Delta V = 0$
ARED	$\Delta V = -\Delta V^*/5$
	$\Delta V = -\Delta V^*/3$
	$\Delta V = -\Delta V^*/2$
	$\Delta V = -\Delta V^*$
ED	$\Delta V^{**} = \Delta V \rightarrow$ 90% LCD
	$\Delta V = \Delta V^{**}/2$
	$\Delta V = \Delta V^{**}/3$
	$\Delta V = \Delta V^{**}/5$

Under ED conditions, the maximum external voltage corresponds to a current density around ~90% of the limiting current density (LCD). The limiting current was estimated by an empirical correlation derived from our own experimental data reported in a previous work [46]. The feed pressure in the RO stage was suitably modified in order to reach the concentration target and, at the same time, maximise the water recovery. In the hybrid systems, the RO modules were selected between SEAMAXX and BW30HR-440i, depending on the RO feed concentration.

3.2. Stand-alone SWRO

In order to properly evaluate the performance of the hybrid systems, a comparison with a stand-alone SWRO was performed. For each simulated case, the same RO feed flow rate as in the hybrid case was fixed, but keeping a concentration of 30 g/l. Operating feed pressure was made vary in order to respect the constraint of permeate concentration (< 0.5 g/l) and to obtain the same permeate flow rate of the corresponding case with the hybrid system. The SW30XHR-440i module was selected for the stand-alone SWRO, as it is the only one (among those listed in Table 3) able to operate under all the conditions investigated, without incurring in alarms or exceeding the operating limits (specified in the data sheets or obtained from the ROSA and WAVE software). For the stand-alone SWRO, an efficiency of 0.9 was assumed for the energy recovery device.

3.3. Analysed performance indicators

One of the performance indicators adopted is the net specific energy consumption, i.e. the total energy consumed (by the hybrid process or the stand-alone SWRO) divided by the flow rate of the permeate produced. For comparison purposes, another indicator, the Cost Saving (*CS*) coefficient, has been defined as:

$$CS = \frac{UPC_{SWRO} - UPC_{hybrid}}{UPC_{SWRO}} \cdot 100\% \quad (9)$$

where UPC_{SWRO} and UPC_{hybrid} are the Unit Product Costs (*UPC*) related to the stand-alone SWRO and to the hybrid plant respectively. *UPC* is the sum of the capital cost depreciated over the plant life (*CapC*) and the operating cost (*OpC*) and it can be calculated as:

$$UPC = CapC + OpC \ [€/m^3] \quad (10)$$

where

$$CapC = \frac{\frac{Capital\ cost\ [€]}{Plant\ lifetime\ [y]}}{Plant\ capacity\ \left[{}^{m^3}/_{h}\right] \times Working\ hours\ per\ year\left[{}^{h}/_{y}\right]} \quad (11)$$

and

$$OpC = \frac{Annual\ operating\ cost\ \left[{}^{€}/_{y}\right]}{Plant\ capacity\ \left[{}^{m^3}/_{h}\right] \times Working\ hours\ per\ year\left[{}^{h}/_{y}\right]} \quad (12)$$

Capital costs (*CapC*) associated with RO have been assumed not to change passing from one configuration to the other, including the change in RO module type (Table 3). This RO *CapC* can be neglected for comparison purposes. For (A)RED and ED, *CapC* were calculated as proportional to the membrane area, as quantified in Table 6.

Operating costs (*OpC*) were associated to the net energy consumption, i.e. the algebraic sum of all the energy contributions of a system, considered positive (as shown in Figure 2c) in the case of energy consumed (ARED, ED and RO units) and negative in the case of energy produced (RED unit). Also in this case, *OpC* were simply expressed as proportional to the net energy consumption, as shown in Table 6.

It is worth noting that the calculated *UPC* does not include the capital costs (and operating costs, other than energy consumption) for the RO unit, thus it cannot be seen as the actual cost of product, but as a parameter useful for comparison purposes.

Eight different cost scenarios were studied: the first one was taken as a reference standard case; the others were obtained by considering a higher and a lower value for the energy and the RED/ED plant costs. The scenario with the highest RED/ED plant cost and the lowest energy cost was not considered as it is clearly the least favourably placed for the hybrid system.

Table 6. Assumptions for the economic analysis.

	Scenarios							
	Standard	**2**	**3**	**4**	**5**	**6**	**7**	**8**
Energy cost [€/kWh]	0.15	0.15	0.15	0.3	0.3	0.3	0.08	0.08
RED/ED plant [€/m^2]	20	10	40	20	10	40	20	10
RED/ED plant lifetime	10 years							
Working hours per year	8000 h/year							

4. Results and Discussion

4.1. (A)RED-RO

The first analysis illustrates the operating and performance parameters for the hybrid system (A)RED-RO. In Figure 6a, the power (provided or required) and the current in the (A)RED process are reported as functions of the external voltage. Note that the power contains also the pumping power, associated with pressure losses in the channels. The salt concentration of the pre-diluted stream from the (A)RED process is reported in Figure 6b. The desalination rate reached by the electromembrane pre-treatment increases when going from right to left in the chart, i.e. as the electrical current increases in absolute value. Therefore, the ARED pre-treatment provides a more diluted feed to the RO stage compared to the RED process, with a minimum value (in the range here investigated) of ~9 g/l. Moreover, the dilution degree is lower (i.e. the concentration is higher) in the electromembrane plant with a lower number of cell pairs (Case_A). In fact, for a given external voltage value, Case_A and Case_B are in two different operating conditions and, in particular, Case_B works close to the short-circuit condition (Figure 6a), so that the desalination degree is higher than in Case_A. In addition, the lower amount of ions transported in Case_A is further induced by a lower residence time. Under ARED conditions, Case_A and Case_B would be ideally equivalent, i.e. in Case_A, the current

is higher, while the residence time is lower. However, non-ideal fluxes (osmotic transport and salt diffusion) contributing to dilute the seawater stream have less effect when the residence time is shorter, thus increasing the outlet concentration from the stack in Case_A.

It is worth noting that, due to concentrations lower than 15 g/l achieved at high voltages ($\Delta V = -\Delta V^*/2 \approx -130$ V and $\Delta V = -\Delta V^* \approx -260$ V), the ARED plant configuration of Case_B is coupled to the RO module for brackish water.

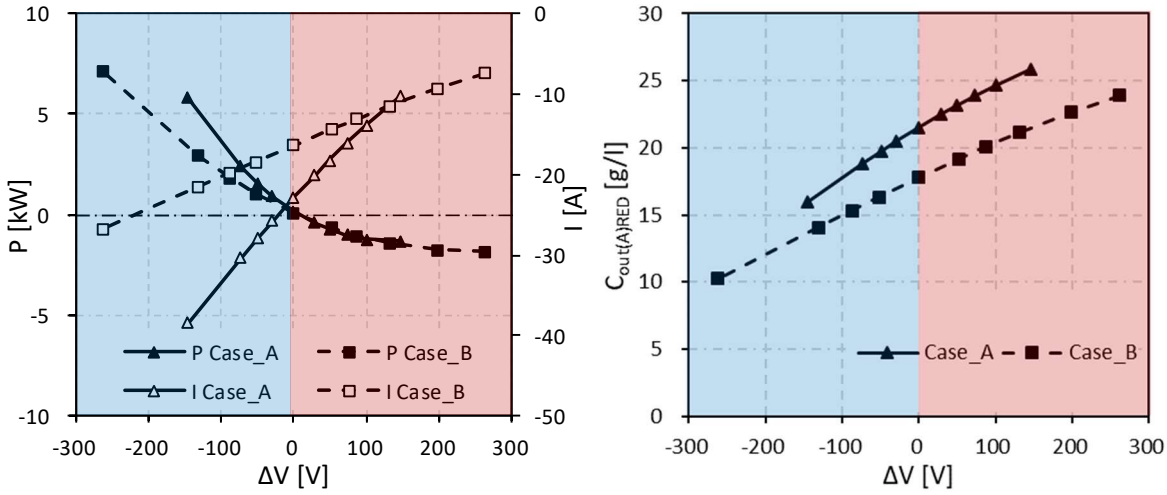

Figure 6. Plots of (a) power and current, (b) outlet concentration of pre-diluted stream from the (A)RED process as a function of the external voltage. Positive voltages are for RED; ΔV=0 is the short-circuit RED; negative voltages are for ARED.

Figure 7 reports the inlet feed pressure in RO, the outlet permeate concentration and the permeate flow rate as functions of the external voltage. The pressure required in the RO unit is in the range from ~35 bar to ~19 bar (while pressure higher than 50 bar are needed in the stand-alone SWRO). Fixing the same product flow rate for the stand-alone SWRO and for the hybrid process, the permeate salt concentration is higher in the two-stage coupled scheme. As the electrical current increases (in absolute value), the reduction of concentration obtained in the pre-treatment (Figure 6b) is reflected in that obtained downstream the RO unit (Figure 7b), and

results in a lower feed pressure in the RO unit (Figure 7a) and in an increase of flow rate (Figure 7c). In particular, passing from the highest to the lowest external voltage, the permeate salt concentration decreases from ~0.38 g/l to ~0.2 g/l, and the flow rate increases from ~120 m^3/day to ~140 m^3/day, with overall recovery from 34% to 41%. In the case of stand-alone SWRO, the salt concentration in the treated water is almost constant and stands at lower values (~0.1 g/l).

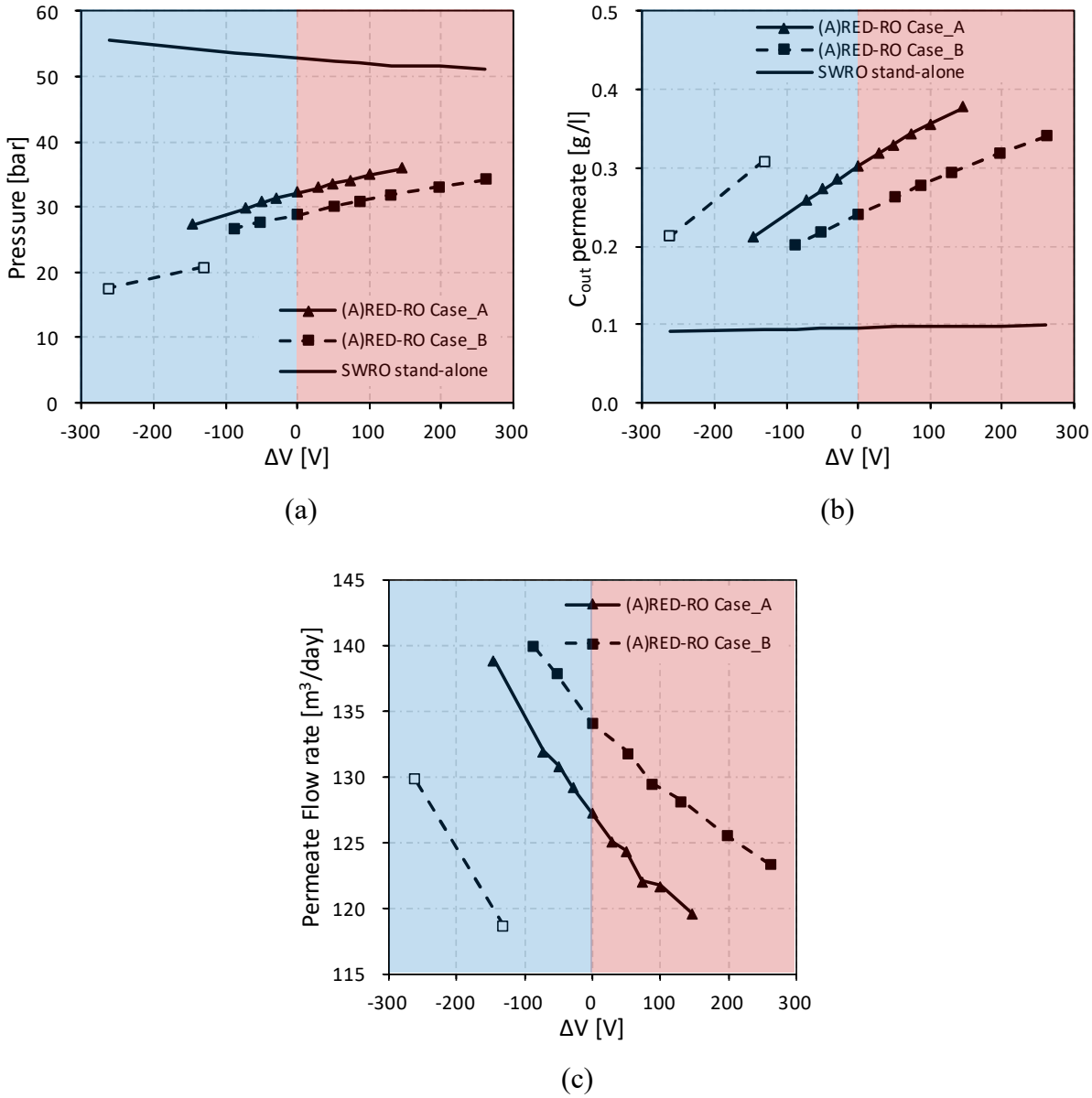

Figure 7. Plots of (a) the feed pressure in RO, (b) outlet permeate concentration and (c) permeate flow rate for the (A)RED-RO integrated process and for the stand-alone SWRO as a function of the external voltage. In Case_B, for two values of the external voltage in the ARED process, the BW30HR-440i RO module was used (empty symbols). The permeate flow rates for the stand-alone SWRO are not reported as they coincide with each single case. Positive voltages are for RED; ΔV=0 is the short-circuit RED; negative voltages are for ARED.

In regard to specific energy consumptions and costs, in Figure 8 the (A)RED-RO hybrid system is compared with the stand-alone SWRO for both Case_A (graphs (a) and (b)) and Case_B (graphs (c) and (d)). Figure 8a and 8c show that, in both Case_A and Case-B, the specific energy consumption of the hybrid process is lower than that of the stand-alone SWRO (which is almost constant, around 1.8 kWh/m^3) in a wide range of voltage, especially for the RED-RO scheme, where the pre-dilution step produces energy and causes a small reduction of energy consumed in the RO.

The minimum energy consumption of the RED-RO coupling is ~1.24 kWh/m^3 in Case_A and ~1.04 kWh/m^3 in Case_B, occurring between conditions of maximum power ($\Delta V = \Delta V^*$, the highest value of voltage considered here) and the short-circuit ($\Delta V = 0$), i.e. $\Delta V = \Delta V^*/2$. In the ARED-RO process, the pre-dilution consumes energy, but further reduces the energy demand of the RO step, resulting in a total energy consumption lower than that of the stand-alone SWRO. The values of total energy consumption are directly reflected in the lower operating costs *OpC*, as shown in Figure 8b and 8d. However, the capital costs *CapC* (assumed proportional to the installed IEM area) make the total costs go up. Note that the slight increase of the *CapC* as the voltage increases, is due to the lower flow rate of permeate produced. Looking at the final unit product cost *UPC*, the range of external voltage where the hybrid system is more cost effective (UPC_{hybrid} equal or lower than the UPC_{SWRO}) is narrower than the range in which an energy saving is obtained. In Case_B, even if the *OpC* is lower than in Case_A, the *CapC* contribution is responsible for a UPC_{hybrid} always higher than the UPC_{SWRO}, making this case not competitive.

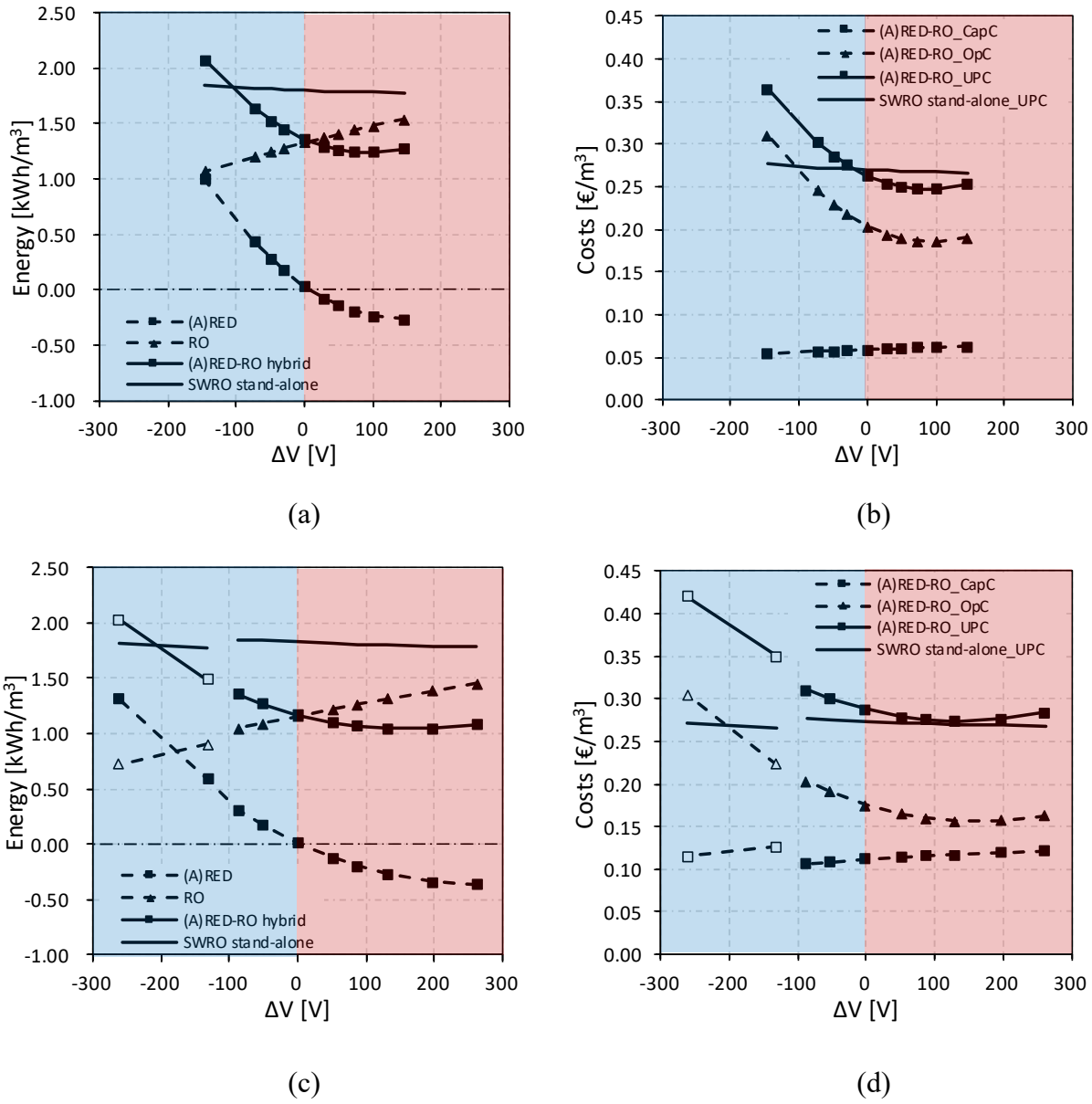

Figure 8. Trends of the energy consumption (positive) or production (negative) per unit volume of permeate produced (left column) and costs (right column) comparison as a function of the external voltage. Graphs (a) and (b) are for the Case_A and graphs (c) and (d) are for the Case_B. In Case_B, for two values of the external voltage in the ARED process, the BW30HR-440i RO module was used (empty symbols). Positive voltages are for RED; ΔV=0 is the short-circuit RED; negative voltages are for ARED. These results were obtained in the standard scenario.

The competitiveness of the two cases with respect to the stand-alone SWRO, can be easily highlighted by using the cost saving *CS* coefficient (Eq. 9) reported in Figure 9 as a function of the external voltage. For any absolute value of the voltage, the RED-RO coupling is cheaper

than the ARED-RO one, thanks to the energy produced by the RED process, along with the energy saved in the following RO step. The cost saving exhibits a maximum under the RED process at an intermediate condition between the maximum power and the short-circuit (ΔV = ΔV*/2) which corresponds to the minimum energy consumption in the hybrid system. In this voltage range, the electromembrane plant configuration of Case_A provides higher cost savings due to the lower *CapC*. Under the conditions simulated and the standard cost scenario, the maximum cost reduction is ~7.5% (with respect to the stand-alone SWRO process). As, observed above from Figure 8, Case_B is not competitive with respect to Case_A because, in a wide range of voltages, it produces or consumes almost the same power than Case_A (Figure 6a) but with a doubled membrane area required and the related *CapC* give a heavy contribution to the final unit product cost *UPC*.

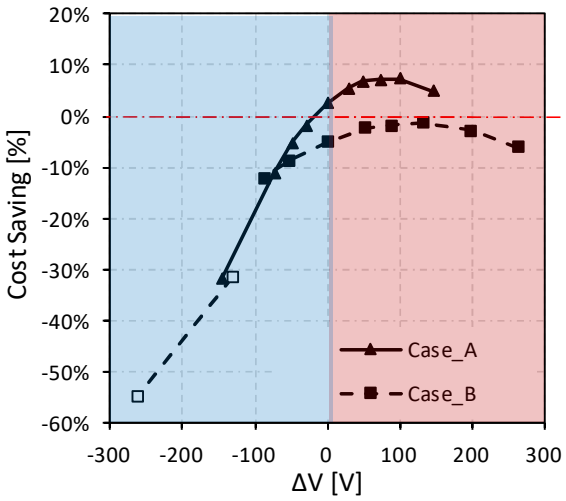

Figure 9. Trend of the Cost Saving of the (A)RED-RO hybrid system as a function of the external voltage. In Case_B, for two values of the external voltage in the ARED process, the BW30HR-440i RO module was used (empty symbols). Positive voltages are for RED; ΔV=0 is the short-circuit RED; negative voltages are for ARED. These results were obtained in the standard cost scenario.

The cost saving may significantly change with the cost of energy and of RED/ED plant. Figure 10 reports the results relevant to the eight different cost scenarios (declared in Table 6) for Case_A only. In scenario 5, with low RED/ED plant cost and high energy cost, the highest values of cost saving are obtained, with a maximum of ~25%, and positive values of *CS* in almost the whole range of voltage. Scenarios 2 and 4 give the same results and provide cost saving values slightly lower than scenario 5. The standard scenario but also scenarios 6 and 8, in which the costs are for both RED/ED plant and energy the highest and lowest respectively, still provide positive cost saving values but in a narrower range of voltage. In these cases the maximum cost saving is ~7.5%. Cases in which the energy cost decreases but the RED/ED plant cost is kept standard, or also the cases in which the RED/ED plant cost increases and the standard energy cost is kept constant, as in scenarios 3 and 7, favour the competitiveness of the stand-alone SWRO desalination for any voltage applied.

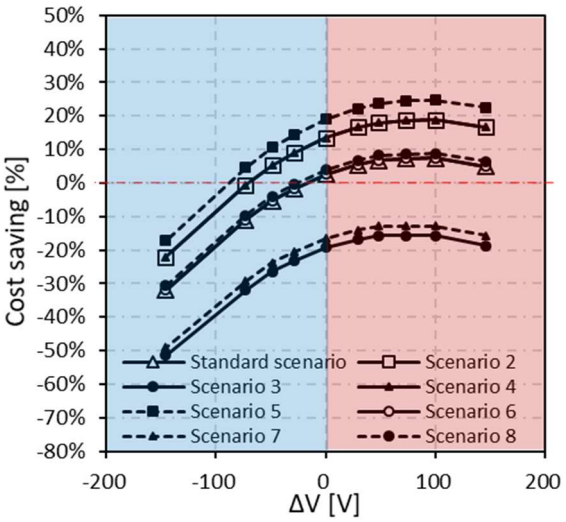

Figure 10. Trend of the Cost Saving as a function of the external voltage for eight costs scenarios. Positive voltages are for RED; ΔV=0 is the short-circuit RED; negative voltages are for ARED. These results were obtained for Case_A.

4.2. ED-RO

In the case of the ED-RO hybrid system, the pre-dilution is achieved by applying ED to the feed seawater, thus removing some of the salt before the stream enters the RO unit. Power required and electrical currents for this case are reported in Figure 11a, while the salt concentration of the pre-diluted stream is reported in Figure 11b, both as a function of the external voltage. As the applied voltage increases, the electrical current increases, thus boosting the pre-dilution, achieving a minimum concentration of ~9 g/l. As in the case of the ARED treatment, Case_A and Case_B differ only due to the effect of non-ideal phenomena, such as water flux and salt flux through the IEMs. However, in ED these fluxes reduce the current efficiency and, thus, pre-dilution effect.

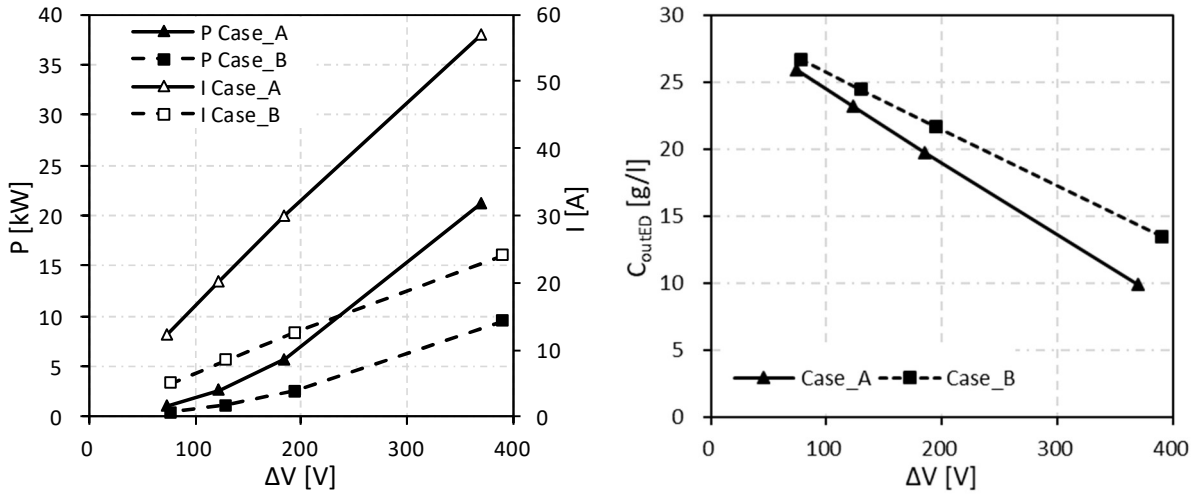

Figure 11. Plots of (a) power and current, (b) outlet concentration of pre-diluted stream from the ED process as a function of the external voltage.

Since the amount of water and salt transported by osmosis and diffusion, respectively, is larger when the residence time is higher, the plant of Case_B attains a lower level of pre-dilution compared to Case_A. With the values of voltage chosen for the simulations (Table 5), the concentration at the outlet of ED falls in a range similar to that of the (A)RED pre-treatment

(Figure 6b). When the highest values of voltage ($\Delta V = \Delta V^{**} \approx$ 370-390 V, corresponding to a current density equal to 90% of the limiting one) are simulated, the low concentrations attained by ED require the use of brackish water RO module.

Figure 12 reports the feed pressure in RO (a), the outlet permeate concentration (b) and the permeate flow rate (c) obtained by the different schemes (both stand-alone SWRO and ED-RO) as a function of the external voltage. The pressure required in the RO step of the hybrid system varies from ~37 bar to ~17 bar, while pressures higher than 50 bar are needed in the stand-alone SWRO. Under the assumption of equal permeate flow rate, the salt concentration in the permeate is almost constant for stand-alone SWRO at 0.1 g/l and is higher in the case of the ED-RO coupling.

This concentration decreases as the voltage increases, and also the flow rate increases. However, in Case_B and at the highest voltage simulated, i.e. $\Delta V = \Delta V^{**}$, these trends are inverted, due to the different performance of the brackish water RO module. The permeate concentration varies from ~0.39 to ~0.21 g/l. The range of the permeate flow rate is narrower than in the (A)RED-RO coupling (~119-131 m^3/day against 120-140 m^3/day, see Figure 7 for comparison). The overall water recovery is also lower, ranging from 34% to 36%.

Details on specific energy consumptions and costs of the ED-RO desalination process are shown in Figure 13.

The energy consumed by the stand-alone SWRO treatment is ~1.75 kWh/m^3 while that consumed by the ED-RO scheme is equal or larger and increases as the voltage increases.

As a matter of fact, the energy demand of the ED pre-treatment exceeds the energy saving in the following RO stage, and this occurs at a larger extent as the voltage increases.

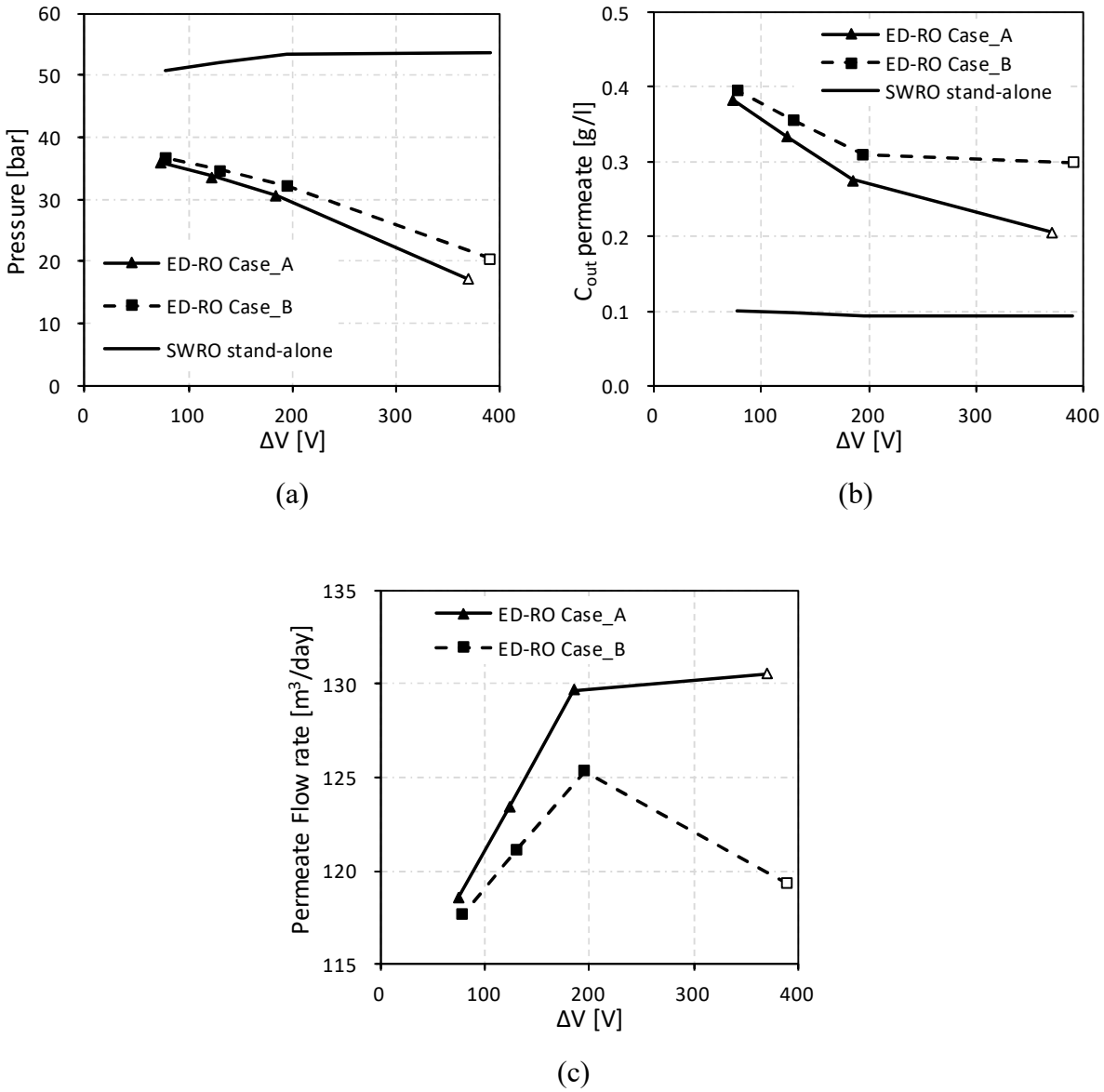

Figure 12. Plots of (a) feed pressure in RO, (b) outlet permeate concentration and (c) permeate flow rate for the ED-RO integrated process and for the stand-alone SWRO as a function of the external voltage. For the highest voltage applied in the ED process, the BW30HR-440i RO module was used (empty symbols). The permeate flow rates for the stand-alone SWRO are not reported as they coincide with each single case.

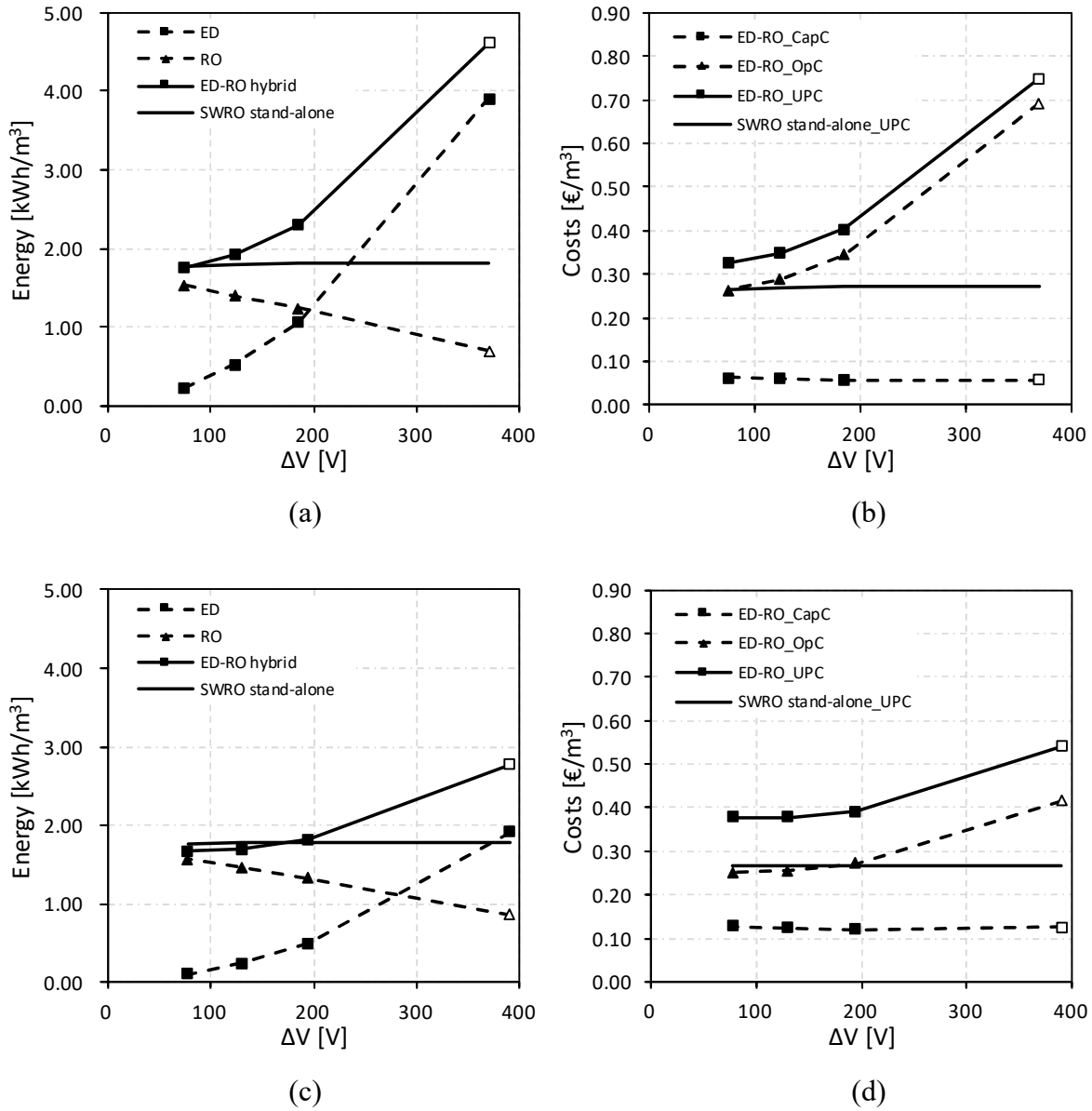

Figure 13. Trends of the energy consumption per unit volume of permeate produced (left column) and costs (right column) comparison as a function of the external voltage. Graphs (a) and (b) are for the Case_A and graphs (c) and (d) are for the Case_B. For the highest voltage applied in the ED process, the BW30HR-440i RO module was used (empty symbols). These results were obtained in the standard scenario.

Translating these results in terms of *OpC* and calculating *CapC* (~0.06 €/m^3 and ~0.12 €/m^3 for Case_A and Case_B respectively), it follows that the total costs considered for the ED-RO process are higher than for the stand-alone SWRO.

These results can be also expressed in terms of cost saving which assumes high negative values as reported in Figure 14. This means that the conditions simulated (plant configuration and operating conditions) are not favourable for the ED-RO coupled scheme in the standard cost scenario, while the stand-alone SWRO and (A)RED-RO (Figure 9) are economically better choices.

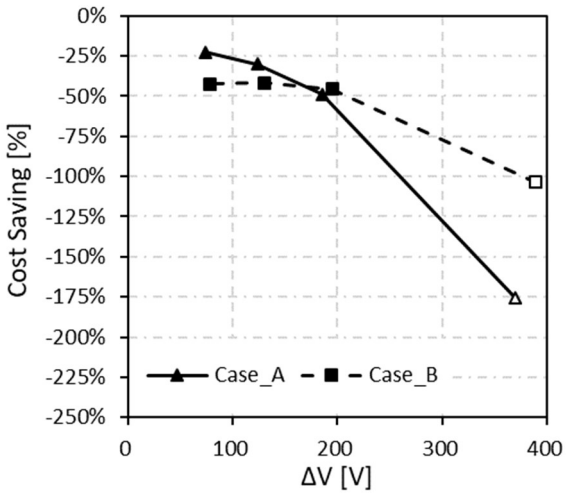

Figure 14. Trend of the Cost Saving of the ED-RO hybrid system as a function of the external voltage. For the highest external voltage in the ED process, the BW30HR-440i RO module was used (empty symbols). These results were obtained in the standard cost scenario.

We can also observe in Figure 14 that up to a voltage of ~180 V (ΔV**/2) the operation by the plant with less cell pairs, i.e. Case_A, is less expensive, while the opposite occurs at higher voltages. At high voltages, the *UPC* in Case_A is heavily affected by the high *OpC* which decreases rapidly when the voltage decreases. In Case_B, the energy consumption and also the *OpC* are less influenced by the voltage and so at low voltages, the *UPC* is affected by the high *CapC*, which is twice the one of Case_A. For these reason, at low voltages, Case_A shows a cost saving higher than Case_B.

The comparison of eight different cost scenarios is reported in Figure 15 for Case_A. Even in the most optimistic cost scenario associated to a reduced price of RED/ED plant and an

increased cost of energy (Scenario 5, Table 6), ED-RO coupling is not economically competitive, despite the cost saving is improved (but still negative).

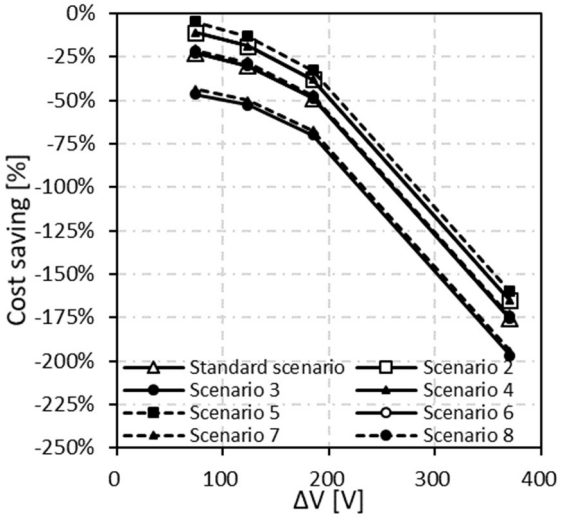

Figure 15. Trend of the Cost Saving as a function of the external voltage for eight costs scenarios. For the highest voltage applied in the ED process, the BW30HR-440i RO module was used (empty symbols). These results were obtained for Case_A.

This behaviour makes the ED-RO process much less interesting than (A)RED-RO, which instead can reduce the desalination cost with respect to the stand-alone SWRO. On the other hand, if the cost of energy was lower or the RED/ED plant cost was higher (pessimistic scenarios 3 and 7), the ED-RO would be even more expensive.

4.3. High performing IEMs

In the previous analysis, we investigated the effect of the RED/ED plant cost (proportional to the membrane area) on the cost saving, i.e. on the competitiveness with respect to the stand-alone SWRO. In this section, we investigate the effect of using high performing IEMs on the system performances. In regard to possible membrane properties improvements, the commercial Fujifilm Type 10 membranes considered in this work (Table 2) have already a very

high permselectivity but they still have a fairly high electric resistance. Considering that the literature reports about membranes with resistances well below 1 Ω cm^2 [54], in order to do a perspective analysis, we considered "high performing" IEMs with electrical resistance equal to a quarter of that of the Fujifilm Type 10 membranes shown in Table 2 [55].

Figure 16a and 16b report the cost saving obtained with the Fujifilm Type 10 membranes and with the high performing IEMs for the (A)RED-RO and the ED-RO hybrid systems respectively. These results were obtained considering only the configuration plant of Case_A, in the standard and best (RED/ED plant cost of 10 €/m2, energy cost of 0.3 €/kWh) cost scenarios. Considering the standard cost scenario (black curves), in the (A)RED-RO hybrid system with high performing IEMs, the maximum cost saving is attained at an external voltage value closer to the short-circuit condition and is of ~16%, i.e. twice the value obtained with Fujifilm Type 10 membranes. It can be also observed that the cost saving with high performing IEMs is not always higher than with Fujifilm Type 10 membranes (Figure 16a) due to the RO stage performance: in assisted RED conditions at high voltages ($\Delta V = -\Delta V^*/2 \approx -65$ V and $\Delta V = -\Delta V^* \approx -130$ V), the cost saving sharply decreases because of the low performance of the BW30HR-440i module that needs to be coupled with the ARED plant when concentrations lower than 15 g/l are achieved.

When high performing IEMs are adopted in the ED-RO hybrid system (Figure 16b), a slight increase in the cost saving can be observed, but it always has negative values. It can therefore be noted that, despite the best performance of the membranes, the ED-RO system remains uncompetitive with respect to the stand-alone SWRO. Finally, looking at the best cost scenarios (red curves), further advantages are recorded for the (A)RED-RO case with high performing IEMs, with a maximum cost saving of ~33%, while in the ED-RO case a nul cost saving is obtained at low voltages.

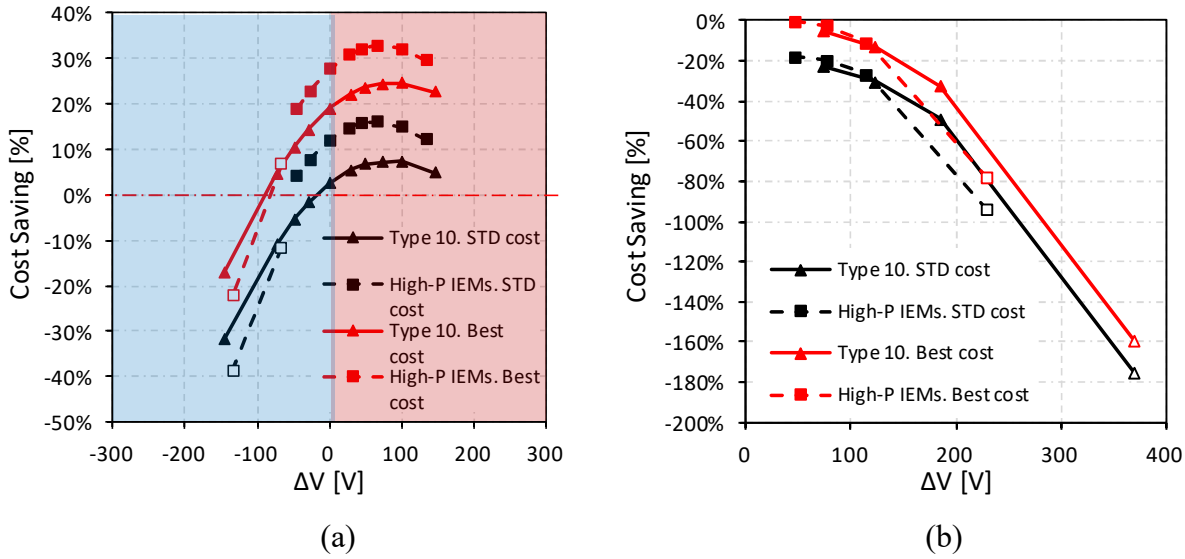

Figure 16. Influence of using reference Fujifilm Type 10 IEMs or high performing IEMs on the cost saving of the (A)RED_RO (a) and of the ED-RO (b) hybrid systems as a function of the external voltage. The empty symbols refer to cases in which the BW30HR-440i module was used. These results were obtained for Case_A, in the standard (black curves) and best (red curves) cost scenarios.

5. Conclusions

In this work, the performance and the costs savings of two coupled processes, (A)RED-RO ((assisted) reverse electrodialysis–reverse osmosis) and ED-RO (electrodialysis–reverse osmosis), were assessed by a validated simulation tool. A sensitivity analysis was performed by changing some design parameters and operating conditions, and considering different cost scenarios.

The (A)RED-RO requires an energy consumption lower than the stand-alone SWRO for a wide range of external voltage in the electromembrane pre-dilution step. Due to capital costs (*CapC*), the cost saving exhibits positive values in a narrower range with a maximum obtained when (i) the external voltage was half that giving the maximum power and (ii) the RED cell pairs are less (2500 rather than 5000), thus reducing *CapC*. A maximum cost saving of ~7.5% can be attained under these conditions and the "standard" cost scenario. In an optimistic cost scenario

with low RED/ED plant costs, proportional to the IEMs costs (10 €/m^2), and high energy cost (0.3 €/kWh) the maximum cost saving can be enhanced to ~24.6%. Therefore, (A)RED-RO coupling is promising, especially in the perspective of a reduced cost of IEMs.

In ED-RO coupling, the energy consumption of the ED pre-treatment exceeds the energy saving of the following RO stage in most of the simulated cases. As a consequence, the total energy demand of the coupled process is larger than that of the stand-alone SWRO (apart from some cases in which it was slightly lower). It follows that cost saving values are negative in all cases (i.e. the cost of desalination by ED-RO is larger than SWRO). Therefore, under the conditions simulated here, ED-RO coupling is not as attractive as (A)RED-RO.

In a perspective analysis with high performing IEMs, the (A)RED-RO system reported a doubled cost saving (~16%) compared to the results obtained with Fujifilm Type 10 membranes in the standard cost scenario. Even with high performing IEMs, the ED-RO system, despite an increase in the cost saving values, was not competitive with respect to the stand-alone SWRO.

Nevertheless, the optimization of plant and operating conditions, along with the IEMs cost abatement, leave room for improvement in the more competitive (A)RED-RO coupling and also ED-RO coupling. Moreover, other scenarios arising from different hybridization schemes can be devised. All this may open the way for the implementation of cost effective conceptual designs for novel systems of seawater desalination.

Acknowledgements

This work has been performed within the REvivED project (Low energy solutions for drinking water production by a Revival of ElectroDialysis system), funded by the European Union's Horizon 2020 Research and Innovation program under Grant Agreement no. 685579 (www.revivedwater.eu).

Nomenclature

Symbol	Quantity	Unit
A	Water permeability constant	l m^{-2} h^{-1} bar^{-1}
B	Salt permeability constant	l m^{-2} h^{-1}
C	Bulk concentration of salt	g l^{-1} (or mol m^{-3} for Eqs. in Appendix)
D_h	Hydraulic diameter	m
D^{SOL}	Salt diffusivity in solution	m^2 s^{-1}
D_{IEM}	Salt diffusive permeability in membrane	m^2 s^{-1}
E	Nernst electric potential per cell pair	V
F	Faraday's constant	C mol^{-1}
f	Friction factor	
G	Mass flow rate	kg s^{-1}
H	Thickness	m
i	Electrical current density	A m^{-2}
I	Electrical current	A
J_W	Water Flux	l m^{-2} h^{-1} (or m s^{-1} for Eqs. in Appendix)
L	Length	m
L_p	Osmotic permeability	m s^{-1} Pa^{-1}
l	Pitch of spacers	m
M	Molar mass	g mol^{-1} (or kg mol^{-1} for Eqs. in Appendix)
N	Salt molar flux	mol m^{-2} h^{-1} (or mol m^{-2} s^{-1} for Eqs. in Appendix)
n_{CP}	Number of cell pairs	-
n_H	Hydration number	-
P	Pressure	bar
Q	Volume flow rate	m^3 s^{-1}
R_G	Gas constant	J mol^{-1} K^{-1}
R_{blank}	Ohmic resistance of electrodes	Ω
Re	Reynolds number	
r	Areal Ohmic resistance per cell pair	Ω m^2

S	Area	m^2
Sh	Sherwood number	-
T	Absolute temperature	K
t	Transport number	-
U	Superficial velocity	$m\ s^{-1}$
W	Width	m
V	Voltage	V
v	Voltage per cell pair	V
y	Co-ordinate along the flow direction	m

Greek symbols

α	Membrane permselectivity	-
γ	Activity coefficient	-
Δ	External voltage	V
η_{BL}	Polarization voltage drop per cell pair	V
θ	Polarization coefficient	-
ν	Kinematic viscosity	$m^2\ s^{-1}$
π	Osmotic pressure	bar
ρ	Density	$kg\ m^{-3}$
σ	Electrical conductivity	$S\ m^{-1}$

Subscripts/superscripts

avg	Average
CONC	Concentrate solution
COUL	Coulombic (proportional to *i*)
DIF	Diffusive
DIL	Dilute solution
d	Permeate duct
E.OSM	Electro-osmotic
f	Feed
i	i-th module in a RO pressure vessel
OSM	Osmotic
p	Permeate

r	Retentate
S	Salt
SC	Short circuit
SOL	Generic solution
W	Water
Ω	Ohmic

Acronyms

AEM	Anion exchange membrane
ARED	Assisted reverse electrodialysis
BWRO	Brackish water reverse osmosis
CapC	Capital costs
CEM	Cation exchange membrane
CFD	Computational fluid dynamics
CS	Cost saving
ED	Electrodialysis
ERD	Energy recovery device
IEM	Ion exchange membrane Generic membrane (AEM/CEM)
LCD	Limiting current density
PV	Pressure vessel
RED	Reverse electrodialysis
RO	Reverse osmosis
OpC	Operating costs
SWRO	Seawater reverse osmosis

References

[1] IDA, IDA Desalination Yearbook 2016 – 2017, (2017).

[2] S.S. Shenvi, A.M. Isloor, A.F. Ismail, A review on RO membrane technology: Developments and challenges, Desalination. 368 (2015) 10–26. doi:10.1016/j.desal.2014.12.042.

[3] L. Henthorne, B. Boysen, State-of-the-art of reverse osmosis desalination pretreatment, Desalination. 356 (2015) 129–139. doi:10.1016/j.desal.2014.10.039.

[4] V.G. Gude, Desalination and sustainability - An appraisal and current perspective, Water Res. 89 (2016) 87–106. doi:10.1016/j.watres.2015.11.012.

[5] R.L. Stover, Seawater reverse osmosis with isobaric energy recovery devices, Desalination. 203 (2007) 168–175. doi:10.1016/j.desal.2006.03.528.

[6] G. Amy, N. Ghaffour, Z. Li, L. Francis, R.V. Linares, T. Missimer, S. Lattemann, Membrane-based seawater desalination: Present and future prospects, Desalination. 401 (2017) 16–21. doi:10.1016/j.desal.2016.10.002.

[7] A. Subramani, M. Badruzzaman, J. Oppenheimer, J.G. Jacangelo, Energy minimization strategies and renewable energy utilization for desalination: A review, Water Res. 45 (2011) 1907–1920. doi:10.1016/j.watres.2010.12.032.

[8] A. Subramani, J.G. Jacangelo, Emerging desalination technologies for water treatment: A critical review, Water Res. 75 (2015) 164–187. doi:10.1016/j.watres.2015.02.032.

[9] B. Peñate, L. García-Rodríguez, Current trends and future prospects in the design of seawater reverse osmosis desalination technology, Desalination. 284 (2012) 1–8. doi:10.1016/j.desal.2011.09.010.

[10] D. Zarzo, D. Prats, Desalination and energy consumption. What can we expect in the near future?, Desalination. 427 (2018) 1–9. doi:10.1016/j.desal.2017.10.046.

[11] S. Lee, J. Choi, Y.G. Park, H. Shon, C.H. Ahn, S.H. Kim, Hybrid desalination processes for beneficial use of reverse osmosis brine: Current status and future prospects, Desalination. 454 (2018) 104–111. doi:10.1016/j.desal.2018.02.002.

[12] N. Voutchkov, Energy use for membrane seawater desalination - current status and trends, Desalination. 431 (2017) 2–14. doi:10.1016/j.desal.2017.10.033.

[13] J. Kim, M. Park, S.A. Snyder, J.H. Kim, Reverse osmosis (RO) and pressure retarded osmosis (PRO) hybrid processes: Model-based scenario study, Desalination. 322 (2013) 121–130. doi:10.1016/j.desal.2013.05.010.

[14] C.F. Wan, T.S. Chung, Techno-economic evaluation of various RO+PRO and RO+FO integrated processes, Appl. Energy. 212 (2018) 1038–1050. doi:10.1016/j.apenergy.2017.12.124.

[15] G. Blandin, A.R.D. Verliefde, C.Y. Tang, P. Le-Clech, Opportunities to reach economic sustainability in forward osmosis-reverse osmosis hybrids for seawater desalination, Desalination. 363 (2015) 26–36. doi:10.1016/j.desal.2014.12.011.

[16] M. Vanoppen, G. Blandin, S. Derese, P. Le Clech, J. Post, A.R.D. Verliefde, Salinity gradient power and desalination, Elsevier Ltd., 2016. doi:10.1016/B978-0-08-100312-1.00009-2.

[17] M. Vanoppen, E. Criel, S. Andersen, A. Prévoteau, A.R.D. Verliefde, Assisted Reverse Electrodialysis: a novel technique to decrease Reverse Osmosis energy demand, AMTA/AWWA Membr. Technol. Conf. Pap. 32 (2016) 1–12. http://hdl.handle.net/1854/LU-7098263.

[18] W. Li, W.B. Krantz, E.R. Cornelissen, J.W. Post, A.R.D. Verliefde, C.Y. Tang, A novel hybrid process of reverse electrodialysis and reverse osmosis for low energy seawater desalination and brine management, Appl. Energy. 104 (2013) 592–602. doi:10.1016/j.apenergy.2012.11.064.

[19] R.K. McGovern, S.M. Zubair, J.H. Lienhard V, The cost effectiveness of electrodialysis for diverse salinity applications, Desalination. 348 (2014) 57–65. doi:10.1016/j.desal.2014.06.010.
[20] R.K. McGovern, A.M. Weiner, L. Sun, C.G. Chambers, S.M. Zubair, J.H. Lienhard V, On the cost of electrodialysis for the desalination of high salinity feeds, Appl. Energy. 136 (2014) 649–661. doi:10.1016/j.apenergy.2014.09.050.
[21] A. Cipollina, G. Micale, Sustainable Energy from Salinity Gradients, Elsevier, 2016.
[22] N.Y. Yip, D.A. Vermaas, K. Nijmeijer, M. Elimelech, Thermodynamic, energy efficiency, and power density analysis of reverse electrodialysis power generation with natural salinity gradients, Environ. Sci. Technol. 48 (2014) 4925–4936. doi:10.1021/es5005413.
[23] A. Ali, E. Drioli, F. Macedonio, Membrane Engineering for Sustainable Development: A Perspective, Appl. Sci. 7 (2017) 1026. doi:10.3390/app7101026.
[24] Y. Mei, C.Y. Tang, Co-locating reverse electrodialysis with reverse osmosis desalination: Synergies and implications, J. Memb. Sci. 539 (2017) 305–312. doi:10.1016/j.memsci.2017.06.014.
[25] K. Kwon, J. Han, B.H. Park, Y. Shin, D. Kim, Brine recovery using reverse electrodialysis in membrane-based desalination processes, Desalination. 362 (2015) 1–10. doi:10.1016/j.desal.2015.01.047.
[26] J. Luque Di Salvo, A. Cosenza, A. Tamburini, G. Micale, A. Cipollina, Long-run operation of a reverse electrodialysis system fed with wastewaters, J. Environ. Manage. 217 (2018) 871–887. doi:10.1016/j.jenvman.2018.03.110.
[27] M. Vanoppen, E. Criel, G. Walpot, D.A. Vermaas, A. Verliefde, Assisted reverse electrodialysis—principles, mechanisms, and potential, Npj Clean Water. 1 (2018) 9. doi:10.1038/s41545-018-0010-1.
[28] H. Strathmann, Ion-Exchange Membrane Separation Processes, First ed., Elsevier, Amsterdam, 2004. doi:10.1007/s13398-014-0173-7.2.
[29] C. Larchet, V.I. Zabolotsky, N. Pismenskaya, V. V. Nikonenko, A. Tskhay, K. Tastanov, G. Pourcelly, Comparison of different ED stack conceptions when applied for drinking water production from brackish waters, Desalination. 222 (2008) 489–496. doi:10.1016/j.desal.2007.02.067.
[30] A. Campione, L. Gurreri, M. Ciofalo, G. Micale, A. Tamburini, A. Cipollina, Electrodialysis for water desalination: A critical assessment of recent developments on process fundamentals, models and applications, Desalination. 434 (2018) 121–160. doi:10.1016/j.desal.2017.12.044.
[31] Y. Tanaka, Ion-exchange membrane electrodialysis program and its application to multi-stage continuous saline water desalination, Desalination. 301 (2012) 10–25. doi:10.1016/j.desal.2012.06.007.
[32] M. Sadrzadeh, T. Mohammadi, Treatment of sea water using electrodialysis: Current efficiency evaluation, Desalination. 249 (2009) 279–285. doi:10.1016/j.desal.2008.10.029.
[33] A.H. Galama, M. Saakes, H. Bruning, H.H.M. Rijnaarts, J.W. Post, Seawater predesalination with electrodialysis, Desalination. 342 (2014) 61–69. doi:10.1016/j.desal.2013.07.012.
[34] S. Thampy, G.R. Desale, V.K. Shahi, B.S. Makwana, P.K. Ghosh, Development of hybrid electrodialysis-reverse osmosis domestic desalination unit for high recovery of product water, Desalination. 282 (2011) 104–108. doi:10.1016/j.desal.2011.08.060.
[35] J.W. Post, H. Huiting, E.R. Cornelissen, H.V.M. Hamelers, Pre-desalination with electro-membranes for SWRO, Desalin. Water Treat. 31 (2011) 296–304. doi:10.5004/dwt.2011.2400.

[36] M. Reig, S. Casas, C. Aladjem, C. Valderrama, O. Gibert, F. Valero, C.M. Centeno, E. Larrotcha, J.L. Cortina, Concentration of NaCl from seawater reverse osmosis brines for the chlor-alkali industry by electrodialysis, Desalination. 342 (2014) 107–117. doi:10.1016/j.desal.2013.12.021.
[37] E.R. Reahl, Reclaiming reverse osmosis blowdown with electrodialysis reversal, Desalination. 78 (1990) 77–89. doi:10.1016/0011-9164(90)80031-6.
[38] Y. Oren, E. Korngold, N. Daltrophe, R. Messalem, Y. Volkman, L. Aronov, M. Weismann, N. Bouriakov, P. Glueckstern, J. Gilron, Pilot studies on high recovery BWRO-EDR for near zero liquid discharge approach, Desalination. 261 (2010) 321–330. doi:10.1016/j.desal.2010.06.010.
[39] R.K. McGovern, S.M. Zubair, J.H. Lienhard V, The benefits of hybridising electrodialysis with reverse osmosis, J. Memb. Sci. 469 (2014) 326–335. doi:10.1016/j.memsci.2014.06.040.
[40] A. Tamburini, G. La Barbera, A. Cipollina, M. Ciofalo, G. Micale, CFD simulation of channels for direct and reverse electrodialysis, Desalin. Water Treat. 48 (2012) 370–389. doi:10.1080/19443994.2012.705084.
[41] F.N. Ponzio, A. Tamburini, A. Cipollina, G. Micale, M. Ciofalo, Experimental and computational investigation of heat transfer in channels filled by woven spacers, Int. J. Heat Mass Transf. 104 (2017) 163–177. doi:10.1016/j.ijheatmasstransfer.2016.08.023.
[42] L. Gurreri, A. Tamburini, A. Cipollina, G. Micale, M. Ciofalo, Performance comparison between overlapped and woven spacers for membrane distillation, Desalin. Water Treat. 69 (2017) 178–189. doi:10.5004/dwt.2017.20236.
[43] L. Gurreri, A. Tamburini, A. Cipollina, G. Micale, M. Ciofalo, Flow and mass transfer in spacer-filled channels for reverse electrodialysis: a CFD parametrical study, J. Memb. Sci. 497 (2016) 300–317. doi:10.1016/j.memsci.2015.09.006.
[44] L. Gurreri, A. Tamburini, A. Cipollina, G. Micale, M. Ciofalo, CFD prediction of concentration polarization phenomena in spacer-filled channels for reverse electrodialysis, J. Memb. Sci. 468 (2014) 133–148. doi:10.1016/j.memsci.2014.05.058.
[45] M. La Cerva, M. Di Liberto, L. Gurreri, A. Tamburini, A. Cipollina, G. Micale, M. Ciofalo, Coupling CFD with a one-dimensional model to predict the performance of reverse electrodialysis stacks, J. Memb. Sci. 541 (2017) 595–610. doi:10.1016/j.memsci.2017.07.030.
[46] M. La Cerva, L. Gurreri, M. Tedesco, A. Cipollina, M. Ciofalo, A. Tamburini, G. Micale, Determination of limiting current density and current efficiency in electrodialysis units, Desalination. 445 (2018) 138–148. doi:10.1016/j.desal.2018.07.028.
[47] J. Schwinge, P.R. Neal, D.E. Wiley, D.F. Fletcher, A.G. Fane, Spiral wound modules and spacers: Review and analysis, J. Memb. Sci. 242 (2004) 129–153. doi:10.1016/j.memsci.2003.09.031.
[48] G. Srivathsan, E.M. Sparrow, J.M. Gorman, Reverse osmosis issues relating to pressure drop, mass transfer, turbulence, and unsteadiness, Desalination. 341 (2014) 83–86. doi:10.1016/j.desal.2014.02.021.
[49] A.H. Haidari, S.G.J. Heijman, W.G.J. van der Meer, Optimal design of spacers in reverse osmosis, Sep. Purif. Technol. 192 (2018) 441–456. doi:10.1016/j.seppur.2017.10.042.
[50] DOW Water & Process Solutions. DOW Water Solution Design Software. Available online: https://www.dow.com/en-us/water-and-process-solutions/resources/design-software (accessed on 5 November 2018), (2018).
[51] D. Chemical, Product Data Sheet DOW FILMTEC ™ BW30HR-440i ™, (2015) 1–2.
[52] D. Chemical, Product Data Sheet DOW FILMTEC ™ SEAMAXX ™, (2017) 1–4.
[53] D. Chemical, Product Data Sheet DOW FILMTEC ™ SW30XHR – 440i ™, (2017) 2–4.

[54] R.A. Tufa, S. Pawlowski, J. Veerman, K. Bouzek, E. Fontananova, G. di Profio, S. Velizarov, J. Goulão Crespo, K. Nijmeijer, E. Curcio, Progress and prospects in reverse electrodialysis for salinity gradient energy conversion and storage, Appl. Energy. 225 (2018) 290–331. doi:10.1016/j.apenergy.2018.04.111.
[55] M. Micari, A. Cipollina, F. Giacalone, G. Kosmadakis, M. Papapetrou, G. Zaragoza, G. Micale, A. Tamburini, Towards the first proof of the concept of a Reverse ElectroDialysis - Membrane Distillation Heat Engine, Desalination. 453 (2019) 77–88. doi:10.1016/j.desal.2018.11.022.
[56] A.A. Sonin, R.F. Probstein, A Hydrodynamic theory of desalination by Electrodialysis, Desalination. 5 (1968) 293–329.
[57] J. Newman, K.E. Thomas-Alyea, Electrochemical Systems, Third edit, John Wiley & Sons, Inc., Hoboken, 2004.
[58] A. Nakayama, Y. Sano, X. Bai, K. Tado, A boundary layer analysis for determination of the limiting current density in an electrodialysis desalination, Desalination. 404 (2017) 41–49. doi:10.1016/j.desal.2016.10.013.
[59] D.W. Green, R.H. Perry, Perry's Chemical Engineers' Handbook, eighth, McGraw-Hill, New York, 2007.
[60] K.S. Pitzer, G. Mayorga, Thermodynamics of electrolytes. II. Activity and osmotic coefficients for 2-2 electrolytes, J. Solution Chem. 3 (1974) 539–546. doi:10.1007/BF00648138.
[61] S.S. Islam, R.L. Gupta, K. Ismail, Extension of the Falkenhagen-Leist–Kelbg Equation to the Electrical Conductance of Concentrated Aqueous Electrolytes, J. Chem. Eng. Data. 36 (1991) 102–104. doi:10.1021/je00001a031.
[62] A.H. Galama, N.A. Hoog, D.R. Yntema, Method for determining ion exchange membrane resistance for electrodialysis systems, Desalination. 380 (2016) 1–11. doi:10.1016/j.desal.2015.11.018.

Appendix: Description of the model for electromembrane processes

The present model for electromembrane processes belongs to the class of multi-scale semi-empirical models [30], where basic data provided by local results of 3-D CFD simulations are merged with one-dimensional higher-scale levels of simulation inside integrated process simulators. One of the basic assumptions of the current version of the model is that the solutions contain only a binary electrolyte (NaCl) and no other ions are present.

In the CFD simulations, continuity, momentum and mass transport equations are solved. The ionic transport is simulated by a convective-diffusive transport equation of the electrolyte. This can be obtained from the Nernst-Planck equations and the mass balances of the two ions of the electrolyte, under the assumption of the local electroneutrality condition in the whole domain [44,56–58]. The electric potential is eliminated from the transport equation, thus simplifying the calculations, requiring only a choice on the boundary condition at the membrane-solution interface for the concentration. Fully developed conditions for flow and concentration are assumed by the Unit Cell approach [44]. CFD results on velocity, pressure and electrolyte concentration fields are then elaborated in order to calculate friction factors and Sherwood numbers. Numerical simulations solving the Laplace equation for the electric potential can also be performed in order to assess the Ohmic resistance [45].

The 1-D process model simulates the cell pair calculating mass balances and the various contributions to the total fluxes of water (osmotic and electro-osmotic) and ions (Coulombic and diffusive) across the membranes. The electric behaviour is described taking into account Ohmic and non-Ohmic contributions to the voltage over the cell pair. Easily accessible experimental data on membrane properties (e.g. salt permeability, permselectivity and electrical resistance) are used. First, the number of cell pairs in the stack, n_{CP}, is left undetermined, and quantities such as electrical potential differences, which are additive with respect to the cell pairs, are referred to a single cell pair. Then, total quantities of the stack can be obtained by

considering its electrical equivalent circuit under the assumption that each cell pair behaves as any other (i.e. flow distribution among the channels and parasitic currents *via* manifolds are neglected), thus multiplying the cell pair voltage drop by n_{CP}. Calculations for the pumping power are also included. The model outcomes are distributed variables (e.g. current density, concentration, fluxes) and performance parameters characterising the stack, such as total current, power consumed or produced and related quantities. Parallel- or counter-flow arrangements can be simulated, while cross-flow layouts requiring at least a 2-D approach are not considered. The model described here is based on the above assumptions and was implemented on different platforms including Excel, gPROMS and G-95 Fortran.

For each channel *SOL* (either *CONC* or *DIL*), the quantity $U^{SOL}=Q^{SOL}/(W^{SOL}H^{SOL})$ (superficial velocity) is adopted as the reference velocity, independent of the presence of spacers or membrane profiles. Consistently, the hydraulic diameter of the generic channel is computed as $2H^{SOL}$, i.e. as the hydraulic diameter of a plane void (spacerless) channel of infinite spanwise extent, and the Reynolds number as $\mathrm{Re}^{SOL}=U^{SOL}\cdot 2H^{SOL}/\nu^{SOL}$. Stack width W and length L are the same for both solutions in parallel- or counter-flow, but may differ in cross-flow. This latter case requires at least a 2-D approach and thus was not considered here.

The following sign conventions are adopted:

- the trans-membrane water flux J_W is positive if directed from diluate to concentrate;
- the trans-membrane salt flux N_S is positive if directed from concentrate to diluate;
- with reference to Figure 2a, which shows a generic cell pair within a stack, the electric current density i is positive if directed from 1 to 2 through the stack (i.e. $i > 0$ for ED, $i < 0$ for RED and ARED); similarly, the external voltage Δv_{ext} (per cell pair) is positive if $V_1>V_2$.

As already mentioned in Section 2.1, according to the working conditions, either electrode (1 or 2) may be positive or negative and may play the role of anode (where oxidation reactions

occur) or cathode (where reduction reactions occur). In particular (see Table 1):

- the positive electrode is the anode in ED and ARED while it is the cathode in RED;
- the negative electrode is the cathode in ED and ARED, while it is the anode in RED.

In Figure A.1 a schematic representation of the ED process is reported as an example. The salt and water fluxes are indicated as well as the electrode signs and the role of the external circuit element. A similar scheme can represent the RED or ARED process, by adjusting salt flux and current directions.

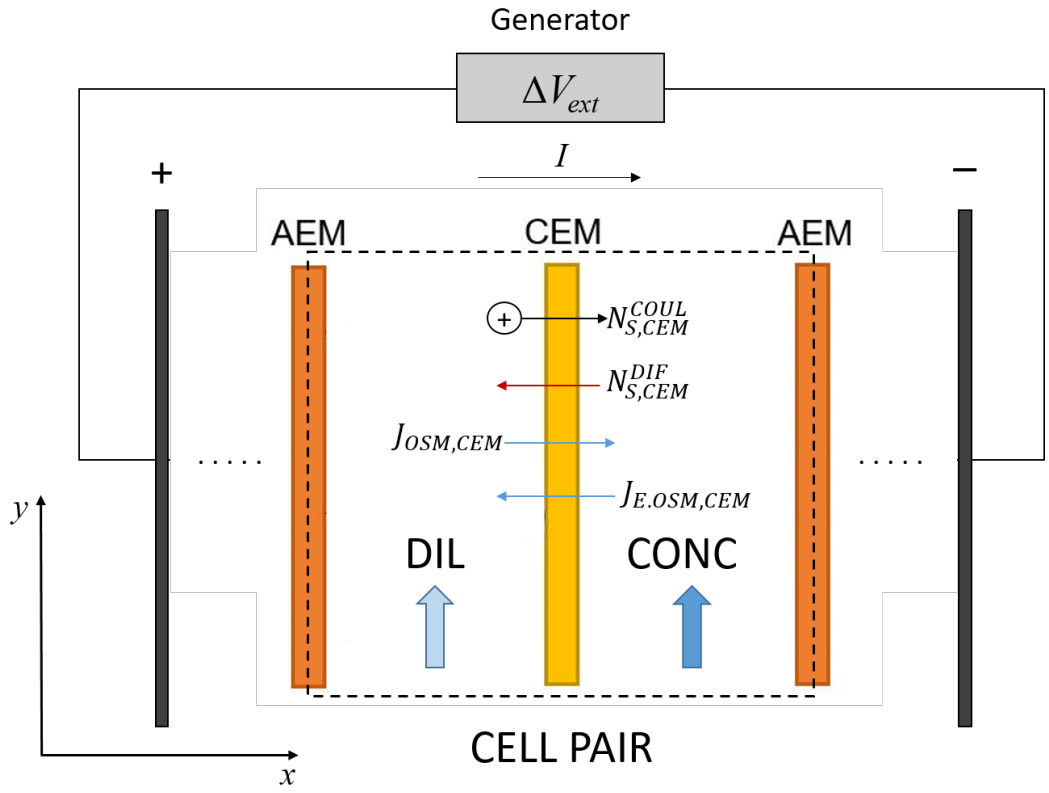

Figure A.1. Schematic representation of the ED process. Salt (Coulombic and diffusive) and water (osmotic and electro-osmotic) fluxes are reported.

Using the above assumptions, the following governing equations may be expressed in a unified form for all working conditions (where fluxes are written for both membranes):

- Equations relating the mass flow rates of water and salt in the generic channel, G_W^{SOL}

and G_S^{SOL} (in kg/s), varying along the axial coordinate y, with the volume flow rate of the solution Q^{SOL} (in m^3/s) and the bulk salt concentration C^{SOL} (in mol/m^3):

$$G_S^{SOL} = M_S C^{SOL} Q^{SOL}; \qquad G_W^{SOL} = \rho^{SOL} Q^{SOL} - G_S^{SOL} \tag{A.1}$$

and their inverses:

$$C^{SOL} = \frac{G_S^{SOL} \rho^{SOL}}{M_S \left(G_W^{SOL} + G_S^{SOL} \right)}; \qquad Q^{SOL} = \frac{G_W^{SOL} + G_S^{SOL}}{\rho^{SOL}} \tag{A.2}$$

in which M_S is the molar mass of salt and ρ^{SOL} is the density of the solution, a function of concentration and temperature [59].

- Local mass balance of water and salt:

$$\frac{dG_W^{CONC}}{dy} = -\frac{dG_W^{DIL}}{dy} = \rho_W J_W W; \qquad \frac{dG_S^{CONC}}{dy} = -\frac{dG_S^{DIL}}{dy} = -M_S N_S W \tag{A.3}$$

in which ρ_W is the pure water density at the working temperature and J_W is the overall trans-membrane water flux in $m^3/(m^2 s)$.

- Expression of J_W as made up of an osmotic and an electro-osmotic contribution:

$$J_W = J_{W,OSM} + J_{W,\,E.OSM} \tag{A.4}$$

- Expression of the osmotic flux:

$$J_{W,OSM} = L_{p,AEM} \left(\pi_{AEM}^{CONC} - \pi_{AEM}^{DIL} \right) + L_{p,CEM} \left(\pi_{CEM}^{CONC} - \pi_{CEM}^{DIL} \right) \tag{A.5}$$

in which $L_{p,IEM}$ is the osmotic permeability of the generic membrane IEM, while π_{IEM}^{SOL} is the osmotic pressure corresponding to the concentration C_{IEM}^{SOL} at the interface of the *SOL* channel with the IEM membrane (so that there are four such terms). Osmotic pressures can be computed as functions of the concentrations by Pitzer's formulae [60].

- Expression of the electro-osmotic flux:

$$J_{W,E.OSM} = -n_H N_S \frac{M_W}{\rho_W} \tag{A.6}$$

where n_H is the hydration number (~7 for NaCl) and N_S is the overall molar salt flux exchanged between the two solutions. Note that in RED and ARED the electro-osmotic water flux is always opposite to the osmotic one while in ED they are in the same direction.

- Expression of the molar salt flux N_S as made up of a Coulombic and a diffusive component:

$$N_S = N_S^{COUL} + N_S^{DIF} \tag{A.7}$$

- Expression of the Coulombic salt flux N_S^{COUL} as proportional to the current density:

$$N_S^{COUL} = -\left[t_{CEM}^{+} - (1 - t_{AEM}^{-})\right]\frac{i}{F} \tag{A.8}$$

where F is the Faraday constant and $t_{IEM}^{\pm}$ is the transport number of counter-ions (either cations or anions) in the generic membrane IEM (either *CEM* or *AEM*). Monovalent ions are assumed here. Note that this definition is consistent with the sign conventions reported above.

- Expression of the diffusive salt flux:

$$N_S^{DIF} = N_{S,AEM}^{DIF} + N_{S,CEM}^{DIF} = \frac{D_{AEM}}{H_{AEM}}\left(C_{AEM}^{CONC} - C_{AEM}^{DIL}\right) + \frac{D_{CEM}}{H_{CEM}}\left(C_{CEM}^{CONC} - C_{CEM}^{DIL}\right) \tag{A.9}$$

where D_{IEM} is the salt diffusive permeability coefficient in the generic membrane. Note that one always has $N_S^{DIF} \geq 0$.

- Expression of the local Nernst potential E (per cell pair) as a function of the local solution concentrations:

$$E = \left(\alpha_{AEM} + \alpha_{CEM}\right)\frac{R_G T}{F}\ln\frac{\gamma^{CONC}C^{CONC}}{\gamma^{DIL}C^{DIL}} \tag{A.10}$$

in which α_{AEM}, α_{CEM} are the permselectivities of the anion and cation exchange membranes, C^{CONC} and C^{DIL} are the local bulk concentrations of concentrate and diluate, γ^{CONC} and γ^{DIL} are the corresponding activity coefficients, T is the absolute temperature and R_G is the gas constant. The activity coefficients γ can be estimated as functions of concentration by Pitzer's formulae [60]. Note that, by this definition, one always has $E \geq 0$.

- Relation between the local current density i and the different potentials:

$$i = \frac{\Delta v_{ext} - E \pm \eta_{BL}}{r_\Omega + R_{blank} / n_{CP}} \tag{A.11}$$

in which η_{BL} is the non-Ohmic drop of E in a cell pair due to the presence of four concentration boundary layers; in the model, it is treated as intrinsically positive in all cases, but the "-" sign applies in the case of ED while the "+" sign applies in the case of (A)RED. Note that the presence of diffusion boundary layers always reduces the absolute value of the electric current. Also, r_Ω is the areal Ohmic resistance of channels and membranes in a cell pair, and R_{blank} is the areal Ohmic resistance of the electrode compartments. Note that in ED one has $\Delta v_{ext} > E + \eta_{BL}$ and thus $i > 0$, whereas in (A)RED one has $\Delta v_{ext} < E - \eta_{BL}$ and thus $i < 0$.

- Expression of the non-Ohmic polarization voltage drop η_{BL} as the sum of four terms, one for each of the four solution-membrane interfaces in a cell pair:

$$\eta_{BL} = \eta_{AEM}^{CONC} + \eta_{CEM}^{CONC} + \eta_{AEM}^{DIL} + \eta_{CEM}^{DIL} \tag{A.12}$$

- Expression of the contribution η_{IEM}^{SOL} at the generic interface:

$$\eta_{IEM}^{SOL} = -\alpha_{IEM} \frac{R_G T}{F} \ln\left(\vartheta_{IEM}^{SOL}\right) \tag{A.13}$$

in which ϑ_{IEM}^{SOL} is the polarization coefficient, defined as

$$\vartheta_{IEM}^{SOL} = \min\left\{C_{IEM}^{SOL} / C^{SOL}, C^{SOL} / C_{IEM}^{SOL}\right\} \tag{A.14}$$

so that ϑ_{IEM}^{SOL}<1 in all cases. In the limit of perfect mixing, one has $\vartheta_{IEM}^{SOL} \to 1$ and $\eta_{IEM}^{SOL} \to 0$.

Each of the polarization coefficients ϑ is related to a Sherwood number

$$\mathrm{Sh}_{IEM}^{SOL} = \left|\frac{N_{S,IEM}}{C^{SOL} - C_{IEM}^{SOL}}\right| \cdot \frac{2H^{SOL}}{D^{SOL}} \tag{A.15}$$

in which $2H^{SOL}$ is the hydraulic diameter of the channel occupied by the solution *SOL* and D^{SOL} is the salt diffusivity in solution *SOL*. $N_{S,IEM}$ is the net (Coulombic + diffusive) salt flux through membrane IEM, necessarily identical on its two opposite IEM-*CONC* and IEM-*DIL* faces and also identical to the salt flux at the interface between IEM and the generic solution *SOL* as seen from the solution side. $N_{S,IEM}$ can be written as:

$$N_{S,IEM} = N_{S,IEM}^{COUL} + N_{S,IEM}^{DIF} \tag{A.16}$$

in which the Coulombic contribution can be evaluated from the transport numbers of the counter-ion in the membrane IEM and in the adjacent solution *SOL*, $t_{IEM}^{counter}$, $t_{SOL}^{counter}$:

$$N_{S,IEM}^{COUL} = -\left(t_{IEM}^{counter} - t_{SOL}^{counter}\right)\frac{i}{F} \tag{A.17}$$

and the diffusive contribution is

$$N_{S,IEM}^{DIF} = \frac{D_{IEM}}{H_{IEM}}\left(C_{IEM}^{CONC} - C_{IEM}^{DIL}\right) \tag{A.18}$$

Note that the total molar salt flux N_S exchanged between the two solutions, Eq. (A.7), is the sum of $N_{S,AEM}$ and $N_{S,CEM}$, as can be verified by using Eqs. (A.8) and (A.9). From the above definitions one has, after some manipulations:

$$\vartheta_{IEM}^{CONC} = \min(X, 1/X) \text{ where } X = 1 - \frac{N_{S,IEM}}{\mathrm{Sh}_{IEM}^{CONC}} \frac{2H^{CONC}}{D^{CONC} C^{CONC}}; \quad \text{(A.19)}$$

$$\vartheta_{IEM}^{DIL} = \min(Y, 1/Y) \text{ where } Y = 1 + \frac{N_{S,IEM}}{\mathrm{Sh}_{IEM}^{DIL}} \frac{2H^{DIL}}{D^{DIL} C^{DIL}} \quad \text{(A.20)}$$

which hold for all operating conditions (ED, RED, ARED). The advantage of using the Sherwood number is that, unlike ϑ, Sh depends only on geometric configuration, Reynolds number and Schmidt number, but not on the specific values of the concentrations and of the current density. For complex geometries (e.g. spacer-filled channels), Sh can be computed by fully 3-D simulations using the CFD code.

- Expressions for the Ohmic areal resistance r_Ω of a cell pair. With void (spacerless) channels and planar membranes, this can simply be computed as the series of four areal resistances:

$$r_\Omega = r^{CONC} + r^{DIL} + r^{AEM} + r^{CEM} \quad \text{(A.21)}$$

The areal Ohmic resistance r^{SOL} of a *void* (spacerless) solution-filled channel is simply

$$r^{SOL} = \frac{H^{SOL}}{\sigma^{SOL}} \quad \text{(A.22)}$$

The electrical conductivity σ of each solution is a function of its bulk concentration C and can be evaluated by Islam's correlations [61]. In regard to the areal Ohmic resistance of the membranes, recent measurements, presented by Galama *et al.*[62], suggest that for any given membrane it depends on the diluate concentration.

In the presence of spacers and/or profiled membranes, more complex expressions are necessary for r_Ω. Details are given in [45].

The above set of equations was cast into a finite difference algorithm providing either outlet concentrations and space-dependent current density for any given voltage at the electrodes, or outlet concentrations and voltage at the electrodes for any given (mean) current density.

Current-voltage curves can thus be built and quantities such as current efficiency or power density can be computed.

In particular, for parallel flow, Eqs. (A.3) are integrated starting from known inlet concentrations. An iterative approach is required because η_{BL} depends on the salt fluxes $N_{S,IEM}$ *via* Eqs. (A.12)-(A.13) and (A.19)-(A.20), and thus on the current density i *via* Eq. (A.17), but in its turn i depends on η_{BL} *via* Eq. (A.11). The case of counter-current flow is treated by a further, "outer" iterative procedure between the inlet and outlet concentrations of the diluate channel [45].